nccrFOAM suite: Nonlinear coupled constitutive relation solver in the OpenFOAM framework for rarefied and microscale gas flows with vibrational non-equilibrium

Tapan K. Mankodi[a], Omid Ejtehadi[b], Tushar Chourushi[c,d], Amin Rahimi[e], R. S. Myong[c,*]

[a] *Department of Mechanical Engineering, Indian Institute of Technology Guwahati, Guwahati, Assam, 781039, India*
[b] *Institute for Materials and Processes, School of Engineering, University of Edinburgh, Sanderson Building, King's Buildings Robert Stevenson Road, Edinburgh, EH9 3FB, UK*
[c] *School of Mechanical and Aerospace Engineering, and ACTRC, Gyeongsang National University, Jinju, Gyeongnam 52828, South Korea*
[d] *School of Aerospace Engineering, AMITY University Maharashtra, Mumbai 410206, India*
[e] *Department of Engineering Science, University West, Trollhttan, Sweden*

*Corresponding author: Tel +82 55 772-1645 (Fax 1580); *myong@gnu.ac.kr*

Abstract

The *nccrFOAM* suite is a collection of nonlinear coupled constitutive relation (NCCR) solvers for rarefied and microscale gas flows with vibrational non-equilibrium, in conjunction with the conservation laws implemented in the foam-extend framework which is an open-source solver with a General Public License (GPL 3). *nccrFOAM* solvers are developed as an extension to the *dbnsTurbFoam* solver by implementing additional algebraic constitutive relations for the non-conserved quantities of the stress tensor and heat flux vector. In contrast to Navier-Stokes-Fourier (NSF) solvers that employ first-order constitutive relations to calculate non-conserved quantities and consequently suffer from obvious shortcomings when simulating gas flows in high non-equilibrium, the second-order NCCR framework presents a novel alternative to simulate rarefied and microscale gas flows in a better and a more intuitive manner. In addition to the solver for monoatomic gases, the solvers are for the first time implemented for diatomic and polyatomic gases with translational-rotational and vibrational degrees of freedom based on second-order constitutive models in a three-dimensional framework. Towards this, a new *foam-extend* library has been written based on the two-temperature formulation to handle the translational-rotational and vibrational modes. The new *foam-extend* solver was validated for several representative problems, and an exhaustive list of tutorials is documented. The solver will certainly benefit the rarefied and microscale gas dynamics and hypersonics communities at large interested in flows involving high degrees of rarefaction, speed, and temperature variations.

Keywords: OpenFOAM; rarefied and microscale gases; second-order constitutive models; two-temperature formulation; vibrational non-equilibrium

PROGRAM SUMMARY

Program Title: nccrFOAM

Licensing provisions: GNU General Public License 3 (GPLv3)

Programming Language: C++

Supplementary material: Shock Structure case files

Nature of the Problem: nccrFoam suite is developed to simulate rarefied and microscale gas flows with vibrational non-equilibrium where the second-order effects of the constitutive models in terms of non-conserved variables such as stress tensor, excess stress (in case of non-monoatomic gases), and heat flux are no longer negligible.

Solution Method: nccrFoam suite is an extension of the *foam-extend* based *dbns* solver where the algebraic relations for non-conserved moments are solved using an alternative numerical method utilizing the tensor operations in the *OpenFOAM* framework. The two-temperature formulation for high-temperature flows was developed with multiple vibrational relaxation models with a new supporting *dbnsv* library.

1. Introduction

Advances in computational fluid dynamics (CFD), along with the advent of high-performance computing, have transformed our understanding of fluid physics and made profound contributions to the study of theoretical and experimental fluid dynamics. The most widely used governing equations for modeling fluid flows are the Navier-Stokes-Fourier (NSF) equations. The higher-order moments, viscous stress and heat flux, appearing in the conservation laws of momentum and energy of the NSF equations are closed using Navier and Fourier's constitutive laws, respectively. These laws are first-order approximations based on the first derivatives of flow velocity and temperature multiplied by viscosity and thermal conductivity, respectively, and are only valid in states not far from thermal non-equilibrium. Most industrial and scientific applications are simulated using NSF-based CFD codes. However, there are important fluid flows for which the application of the NSF equation is questionable. In this work, we are mainly concerned with these applications: rarefied and microscale and high-temperature non-equilibrium gas flows.

Rarefied gas flows—gas flows in a low-density state—are present in a wide range of scientific and technological problems. Such flows can affect hypersonic vehicles flying at very high altitudes and the propulsion systems of spacecraft navigating in space [1]. In addition,

vacuum devices operating on the ground, such as gas deposition manufacturing processes in near-vacuum conditions, are yet another interesting application of rarefied gases.

The flow of systems related to rarefied gases can be classified using the Knudsen number (representing the altitude) and the Mach number (representing the flow speed) [2–4]. Note that at least two non-dimensional parameters—for example, the Reynolds and Mach (or Knudsen and Mach) numbers—are necessary to fully classify the gas flow regimes. The degree of non-equilibrium measured by the product of the Mach number and the Knudsen number (viscous force/pressure) reaches the highest for re-entry vehicles, followed by high hypersonic glider vehicles, and computer hard disk drives. In the case of re-entry vehicles, the degree of thermal non-equilibrium is sufficiently high at an altitude of 60 to 65 km where the maximum heat flux occurs, and so there is a limit to the validity of the NSF theory at higher altitudes.

Microscale gas flows—gas flows associated with micron- or sub-micron-sized devices—exist in many scientific and technological problems today. Some of these flows include internal flows through micro-channels, micro-pumps and micro-turbines, and external flows around micro-particles. In these flows, gas-surface interactions are of the same order or even dominant over the gas-gas bulk interactions, leading to interesting physics, such as velocity slip and temperature jumps on solid surfaces. These applications are also classified as flows away from thermal non-equilibrium due to the small characteristic length of the flow domain.

Hypersonic rarefied gas flows have an additional complication in the form of vibrational non-equilibrium. The kinetic energy in the hypersonic gas flow transforms into thermal energy across a shock structure. The thermal energy is restricted to the translational degree of freedom immediately downstream of the shock front. The ambient gas in Earth's atmosphere is mainly composed of diatomic molecules. In the region further downstream from the shock front, the high-energy gas molecules collide with each other resulting in energy redistribution among the three internal modes (translational, rotational, and vibrational) of energy. The number of collisions required to establish equilibrium between the translational and the vibrational degrees of freedom is considerably higher than those required for the equilibration of translational and rotational degrees of freedom. It is generally assumed that the translational-rotational or simply trans-rotational equilibrium is established instantly and the two modes of internal energy can be combined to give a trans-rotational degree of freedom. In contrast to this, the slower vibrational-translational (VT) relaxation leads to a region in the domain where there is a definite difference in the energy stored in the trans-rotational modes and the

vibrational modes. Park [5] proposed a two-temperature framework to model this non-equilibrium. In this framework, to handle the VT relaxation process, a separate partial differential equation for the vibrational energy is added to the existing NSF conservation laws that contain a non-zero source term.

Various methods are employed to understand the different flow regimes as a function of non-equilibrium parameters (rarefaction and compressibility). They include the zeroth-order Euler equations which are appropriate for gas flows in local thermal equilibrium (LTE), the first-order Navier-Stokes-Fourier equations used in flows near LTE, and higher-order methods for studying flows far from LTE. Other popular particle-based methods are employed to study rarefied gas flows, especially at higher Knudsen numbers, such as the Lattice Boltzmann method (LBM) [6,7] and direct simulation Monte Carlo (DSMC) [8–13]. Several PDE-based higher-order methods have also been reported, such as the Burnett equation [14–16], super-Burnett equations [17–19], R-13 moment equations [20–21], generalized hydrodynamics (GH) [22–26], extended thermodynamics (ET) [27,28] and rationalized extended thermodynamics (RET) [29,30]. Furthermore, various kinetic schemes have been proposed, including the discrete velocity method [31], the unified gas-kinetic scheme [32], the discrete unified gas-kinetic scheme [33], and the gas-kinetic unified algorithm [34]. Recently, a novel solver based on a combination of kinetic flux solver, discrete velocity method, and moment method was also developed to simulate flows from continuum to rarefied regimes at moderate Knudsen number [35].

Compared to the first-order NSF-based CFD algorithms, the PDE-based higher-order methods are more suitable for simulating highly non-equilibrium flows. However, many of these methods have additional theoretical or numerical drawbacks. For example, the Burnett equation uses higher-order derivatives of the flow properties to close the open terms related to viscous stress and heat flux in the constitutive equation. However, the use of higher-order derivatives requires additional boundary conditions that greatly increase the modeling complexity of the method [36]. Moreover, as the degree of thermal non-equilibrium increases, the boundary condition modeling related to gas-surface interaction becomes more important, but an accurate higher-order boundary condition has not been developed so far.

Myong's nonlinear coupled constitutive relations (NCCR) [3,4,37,39–43,44–48], which were systematically derived from the Boltzmann kinetic equation based on Eu's modified moment method [25,26,38] and Myong's closing-last balanced closure [2], are novel

alternatives to previous methods. Firstly, they are derived to fully comply with the second law of thermodynamics by ensuring non-negative entropy production [24,25] under all flow conditions. Secondly, the constitutive equations for the non-conserved quantities in their original formulation are a set of algebraic relations that, although nonlinear and coupled in nature, are simpler than solving the partial differential equations that appear in many of the higher-order methods. The NCCR was initially developed based on the explicit finite volume method (FVM) for one- and two-dimensional flow problems [3,4,37]. The NCCR has been implemented recently into a three-dimensional mixed modal discontinuous Galerkin (DG) framework, where auxiliary variables were introduced to solve the implicit algebraic NCCR of non-conserved variables [39–43]. The NCCR has also been studied by other researchers [44–48] who have used the implicit finite volume method (FVM) as a basic numerical scheme.

Previous higher-order methods have traditionally focused on investigating monoatomic gas flows and have only begun to consider diatomic and polyatomic gas flows rather recently. For instance, in 2015 Ruggeri et al. [29] extended the RET framework beyond the monoatomic gas and developed a relevant theory for polyatomic gases, both in rarefied and dense conditions. On the other hand, Myong and his collaborators have extended the NCCR framework to diatomic and polyatomic gases based on the Boltzmann-Curtiss equation [49,50] and have developed second-order NCCR models since 2004 [37,39–42].

Unlike the original Boltzmann kinetic equation, the Boltzmann-Curtiss kinetic equation additionally introduces the angular momentum and azimuth angle associated with the rotational mode of molecules to the kinetic formulation. In the NCCR framework, the bulk viscosity of diatomic and polyatomic gases was viewed as a quantity directly related to the relaxation time associated with the rotational degrees of freedom. It was shown by McCourt *et al*. [51, p. 276] that the excess normal stress appearing in the conservation law of momentum is equivalent to the difference between the translational and rotational temperatures. Thus, the hydrodynamic equation can be formulated in two ways: either introducing the excess normal stress and keeping the one temperature ($T_{trans\text{-}rot}$) concept or introducing two temperatures (T_{trans} & T_{rot}) but no excess normal stress. The former was employed in Myong's study [37,39–42] because it is a natural extension of the first-order Navier-Fourier constitutive laws, and the one-temperature hydrodynamics is more naturally connected to the laws of thermodynamics.

Recently, Mankodi and Myong [52] developed a new set of governing equations based on the two-temperature ($T_{trans\text{-}rot}$ & T_{vib}) formulation to simulate the second-order effects of

diatomic and polyatomic gases with activated vibrational degrees of freedom and vibrational-transrotational non-equilibrium. The new set of equations included an additional equation of vibrational energy and a constitutive equation of the vibrational heat flux. The constitutive equations of the viscous stress tensor, excess normal stress, transrotational heat flux, and vibrational heat flux showed interesting coupling effects leading to unique nonlinear problems. Moreover, analysis of a strong shock structure highlighted the interplay between the second-order effects in the constitutive relations and the vibrational-transrotational non-equilibrium. Furthermore, the analysis showed that the results of the second-order models were in better agreement with the direct simulation Monte Carlo data when compared with the results of the first-order models, especially in the profiles and slopes of density, velocity, and vibrational temperatures.

The theoretical knowledge required to understand the second-order effects in complex flow situations has a steep learning curve. In addition, the mathematical and computational tasks of solving the complicated algebraic NCCR model are challenging. To this end, an NCCR solver based on an open-source framework will benefit the scientific community and industry working in the study of rarefied and microscale gas dynamics and hypersonics. The present work reports a new NCCR solver based on the openFOAM framework, *nccrFOAM*, developed by extending the *dbnsTurbFoam* solver in a *foam-extend* fork. The *nccrFOAM suite* mainly consists of two solvers: *nccrFOAM* for monoatomic, diatomic, and polyatomic gases at low temperature in the single-temperature ($T_{trans\text{-}rot}$) formulation, and *nccrVibFOAM* for high-temperature diatomic and polyatomic gases with vibrational non-equilibrium, having a provision for a wide range of VT relaxation models in the two-temperature ($T_{trans\text{-}rot}$ & T_{vib}) formulation. Both solvers can simulate gas flows with first and second-order constitutive relations. *To the best of the authors' knowledge, the nccrFOAM suite is the first-of-its-kind solver based on second-order constitutive models developed in an open-source framework to simulate rarefied and microscale gas flows with vibrational non-equilibrium.*

Section 2 explains the derivation of the NCCR models in detail and highlights the novelty of the NCCR method. In Section 3, an alternative algorithm for solving the coupled tensorial and vector constitutive equations is presented and compared with the previous iterative methods. The structure of the *nccrFOAM* solver, its implementation, and details about designing a *nccrFOAM* simulation case are then described in Section 4. In Section 5, the validation of the *nccrFOAM* solver is shown for 1D simulations demonstrating the robustness

of the new solver. Further, shock structure simulations for monoatomic, polyatomic gases with and without vibrational non-equilibrium are performed and their profiles are compared with those obtained using an in-house FVM solver. Moreover, multi-dimensional NCCR simulations are also conducted for three representative flows: 1) a 2D hypersonic flow over a cylinder for monoatomic, diatomic, and polyatomic gases with VT relaxation; 2) a 2D steady-state compressible Poiseuille flow of argon gas through a micro-channel; and 3) a 3D rarefied gas flow associated with the impingement of a nozzle jet onto a surface at near-vacuum condition. The flow properties obtained with the first- and second-order constitutive relations are also briefly discussed. Finally, a summary of the present work along with a remark on future research is provided in Section 6.

2. The second-order NCCR model with vibrational non-equilibrium

2.1. *Derivation of the second-order NCCR model with vibrational non-equilibrium*

Generally, diatomic and polyatomic gas molecules are in their vibrational ground states at standard temperature conditions. At lower temperatures, the governing equation for understanding the statistics of diatomic and (linear) polyatomic gas flows at relatively low temperatures is given by the Boltzmann-Curtiss kinetic equation [49] which has additional dependent variables in the form of angular momentum and azimuthal angle. At higher temperatures, the vibrational modes are activated, and the molecules can reside in one of the higher vibrational quantum levels. The statistics for polyatomic gases at such high temperatures can neither be modeled using the Boltzmann kinetic equation nor the Boltzmann-Curtiss kinetic equation.

Recently, a modified Boltzmann-Curtiss kinetic equation was proposed by Mankodi and Myong [52] for such diatomic and polyatomic gas flows containing molecules in higher vibrational levels:

$$\frac{\partial f_i}{\partial t} + \mathbf{v}\cdot\nabla f_i + \mathbf{L}\cdot\nabla_r f_i = \sum_j \sum_k \sum_l \int dv_j \int d\Omega W(i, j, | k^*, l^*; \Omega)(f_k^* f_l^* - f_i f_j) = \sum_j C[f_i, f_j]. \tag{1}$$

Here f_i is the distribution function of the population of molecules at the i^{th} vibrational level. The variables r_i, $\mathbf{v}_i$, $\mathbf{L}_i$, and t represent the position, velocity, angular velocity, and time, respectively. Ω is the solid angle. For simplicity, the subscripts are dropped, since the molecules essentially belong to the same species. The terms with an asterisk in the superscripts

represent the post-collision states. The term $W(i, j, | k^*, l^*; \Omega)$ is the probability of the interaction among molecules in the i^{th} and j^{th} vibrational levels undergoing inelastic collision to the k^{th} and l^{th} vibrational quantum levels. The summation over the j^{th}, $k^{\text{th,}}$ and l^{th} vibrational levels ensures that interactions over all possible post-collision combinations of vibrational levels are handled.

Upon introducing the statistical formula of conserved and non-conserved variables, differentiating the statistical definitions of total density, total momentum and total energy with time, combining them with the modified Boltzmann-Curtiss kinetic equation, and invoking the collision invariance of mass, momentum, and energy, the following conservation laws for mass, momentum, and energy are obtained:

$$\frac{\partial}{\partial t}\begin{bmatrix}\rho\\ \rho\mathbf{u}\\ \rho e\end{bmatrix}+\nabla\cdot\begin{bmatrix}\rho\mathbf{u}\\ \rho\mathbf{u}\mathbf{u}+p\mathbf{I}\\ (\rho e+p)\mathbf{u}\end{bmatrix}+\nabla\cdot\begin{bmatrix}0\\ \boldsymbol{\Pi}+\Delta\mathbf{I}\\ (\boldsymbol{\Pi}+\Delta\mathbf{I})\cdot\mathbf{u}+\mathbf{Q}+\mathbf{Q}_v\end{bmatrix}=0, \tag{2}$$

where ρ is the density, $\mathbf{u}$ is the average velocity, p is the hydrostatic pressure, e is the total energy density, $\boldsymbol{\Pi}$ is the viscous shear stress tensor, Δ is the excess normal stress, $\mathbf{Q}$ is the heat flux for trans-rotational energy, and $\mathbf{Q}_v$ is vibrational heat flux. T, T_v are trans-rotational temperature and the temperature associated with the vibrational energy of gas molecules, respectively. The pressure p and temperature T are related through the equation of state $p=\rho RT$. In contrast, because the vibrational energy (e_v) is not a collisional invariant, the vibrational energy equation has a non-vanishing collisional term as follows,

$$\frac{\partial(\rho e_v)}{\partial t}+\nabla\cdot(\rho e_v\mathbf{u})+\nabla\cdot\mathbf{Q}_v=\dot{\omega}_v. \tag{3}$$

Here the source term on the right-hand side, $\dot{\omega}_v$, is defined as

$$\dot{\omega}_v=\frac{1}{\tau_v}\left(\rho e_v(T)-\rho e_v(T_v)\right),$$

where τ_v is a relaxation factor.

The source term on the right-hand side represents the trans-rotational and vibrational non-equilibrium and is dependent on the vibrational-trans-rotational relaxation factor (τ_v). There are several models for estimating V-T relaxation times, such as the constant collision factor model, the Millikan-White (MW) model [53], the Millikan-White-Park (MWP) model [5], and

the SSH model [54]. The constant collision factor model employs a non-dimensional relaxation parameter, and the V-T relaxation time is simply a product of the relaxation parameter and the local mean collision time. The constant collision factor model, MW, and the MWP vibrational relaxation models are implemented in the new *nccrFOAM.*

The constitutive equations for the four undetermined variables—viscous shear stress tensor, excess normal stress, heat flux, and vibrational heat flux—are derived similarly: first differentiating the statistical definition of the variables with time and then combining them with the modified Boltzmann-Curtiss kinetic equation,

$$
\begin{aligned}
&\rho\frac{d(\boldsymbol{\Pi}/\rho)}{dt}+\nabla\cdot\boldsymbol{\psi}^{(\boldsymbol{\Pi})}+2[\boldsymbol{\Pi}\cdot\nabla\mathbf{u}]^{(2)}+2(p+\Delta)[\nabla\mathbf{u}]^{(2)}=\boldsymbol{\Lambda}^{(\boldsymbol{\Pi})},\\
&\rho\frac{d(\Delta/\rho)}{dt}+\nabla\cdot\boldsymbol{\psi}^{(\Delta)}+2\gamma'(\boldsymbol{\Pi}+\Delta\mathbf{I}):\nabla\mathbf{u}+\frac{2}{3}\gamma' p\nabla\cdot\mathbf{u}=\boldsymbol{\Lambda}^{(\Delta)},\\
&\rho\frac{d(\mathbf{Q}/\rho)}{dt}+\nabla\cdot\boldsymbol{\psi}^{(\mathbf{Q})}+\boldsymbol{\psi}^{(\mathbf{P})}:\nabla\mathbf{u}+\mathbf{Q}\cdot\nabla\mathbf{u}+\frac{d\mathbf{u}}{dt}\cdot\boldsymbol{\Pi}+\boldsymbol{\Pi}\cdot\nabla(C_pT)+(p+\Delta)\nabla(C_pT)=\boldsymbol{\Lambda}^{(\mathbf{Q})},\\
&\rho\frac{d(\mathbf{Q}_v/\rho)}{dt}+\nabla\cdot\boldsymbol{\psi}^{(\mathbf{Q}_v)}+\mathbf{Q}_v\cdot\nabla\mathbf{u}+\boldsymbol{\Pi}\cdot\nabla(C_{p,v}T_v)+(p+\Delta)\nabla(C_{p,v}T_v)=\boldsymbol{\Lambda}^{(\mathbf{Q}_v)},
\end{aligned}
\tag{4}
$$

where γ', C_p and $C_{p,v}$ are the ratio of the rotational specific heat capacity energy to specific heat capacity at constant volume, defined as $\gamma'=(5-3\gamma)/2$, specific heat capacity at constant pressure, and vibrational specific heat capacity at constant pressure, respectively.

In the constitutive equations (4), $\boldsymbol{\psi}^{(\boldsymbol{\Pi},\Delta,\mathbf{Q},\mathbf{P},\mathbf{Q}_v)}$ represent the open high-order terms of the viscous shear stress, the excess normal stress, the heat flux, the stress, and the vibrational heat flux, respectively. $\boldsymbol{\Lambda}^{(\boldsymbol{\Pi},\Delta,\mathbf{Q},\mathbf{Q}_v)}$ on the right-hand side of Eq. (4) represent the dissipation in the non-conserved quantities which is attributed to the collisional operator in the kinetic equation. At this point, it should be mentioned that the constitutive equations (4) are an exact consequence of the modified Boltzmann-Curtiss equation (1) and are thus capable of capturing the whole flow physics if they are provided with accurate closure on the open higher-order terms $\boldsymbol{\psi}^{(\boldsymbol{\Pi},\Delta,\mathbf{Q},\mathbf{P},\mathbf{Q}_v)}$ and $\boldsymbol{\Lambda}^{(\boldsymbol{\Pi},\Delta,\mathbf{Q},\mathbf{Q}_v)}$.

Among closure theories, we employ the so-called "*closing-last balanced closure*," which was proposed by Myong in 2014 [2] from a keen observation of the essence of the closure problem in a complex system: when closing open terms, the number of places to be closed is two (movement and interaction), rather than one (movement only) and thus the order of approximations in handling the two terms—kinematic (movement) $\boldsymbol{\psi}^{(\boldsymbol{\Pi},\Delta,\mathbf{Q},\mathbf{P},\mathbf{Q}_v)}$ and dissipation

(interaction) $\boldsymbol{\Lambda}^{(\boldsymbol{\Pi},\Delta,\mathbf{Q},\mathbf{Q}_v)}$ terms—must be the same to satisfy balancing; for instance, the second-order closure for both terms, $\boldsymbol{\psi}_{2nd}^{(\boldsymbol{\Pi},\Delta,\mathbf{Q},\mathbf{P},\mathbf{Q}_v)}$ and $\boldsymbol{\Lambda}_{2nd}^{(\boldsymbol{\Pi},\Delta,\mathbf{Q},\mathbf{Q}_v)}$.

In this balanced closure theory, third-order closure for $\boldsymbol{\Lambda}^{(\boldsymbol{\Pi})}$ in the constitutive equation of viscous shear stress may not be essential; in fact, unbalanced higher-order closure in the moment method may not provide improved solutions as promised, especially in the case of a high Mach number shock structure problem [2]. Note that the present closure is not the same as Eu's closure [25,26], and the significance of the difference—in the case of the constitutive equations of heat flux, $\nabla\cdot\boldsymbol{\psi}^{(\mathbf{Q})}+\boldsymbol{\psi}^{(\mathbf{P})}:\nabla\mathbf{u}=0$ vs $\boldsymbol{\psi}^{(\mathbf{Q})}=\boldsymbol{\psi}^{(\mathbf{P})}=0$—should not be overlooked. The present balanced closure effectively resolves the weakness of Eu's closure, like $\boldsymbol{\psi}^{(\mathbf{P})}\left(\equiv\left\langle m\mathbf{CCC}f\right\rangle\right)=0$, which was strongly criticized by mathematicians and physicists for its inconsistency, i.e., that the term $\left\langle m\mathbf{CCC}f\right\rangle$ cannot be zero in general, especially in strong thermal non-equilibrium.

Closing the dissipation $\boldsymbol{\Lambda}^{(\boldsymbol{\Pi},\Delta,\mathbf{Q},\mathbf{Q}_v)}$ terms requires special care as well because it is directly related to the energy dissipation accompanying the irreversible processes, the calortropy production in the system, and the second law of thermodynamics. We employ the so-called "*cumulant expansion method*," which was developed by Eu in 1980 [23,26] based on a canonical distribution function in the exponential form, after recognizing the logarithmic form of the non-equilibrium entropy production. Unlike conventional polynomial expansions, the cumulant expansion of the distribution function in the series of the 1st-mean, 2nd-variance, 3rd-skewness, 4th-excess (or kurtosis), etc., assures the non-negativity of the distribution function regardless of the level of approximations.

Furthermore, the temporal dependence in the constitutive equations (4) can be neglected, owing to the very short relaxation times of the non-conserved variables, being on the order of 10^{-10} second [3,25], compared to those for conserved variables and the characteristic times of the flow process. This so-called adiabatic approximation simplifies the partial differential-type constitutive equations into a set of algebraic equations in the Lagrangian frame, which greatly reduces the numerical complexities involved in solving the constitutive equations.

Further simplifications can be made to the constitutive equations (4) [3]. Pure convective terms present in the constitutive equations are negligible because they are strictly zero in the one-dimensional velocity-shear flow and their contributions are not large compared to the other

terms. Also, the $(\mathbf{Q},\mathbf{Q}_v)\cdot\nabla\mathbf{u}$ terms in the constitutive equations of heat flux can be omitted because they have the same property (heat flux times viscous stress) as the $\mathbf{\Pi}\cdot\nabla(C_pT,C_{p,v}T_v)$ terms.

Once these tenets—Myong's closing-last balanced closure, and Eu's cumulant expansion based on the canonical distribution function in the exponential form to the explicit calculation of the dissipation term—are applied to the constitutive equations (4) and after introducing the adiabatic approximation and aforementioned additional simplifications, the following *two-temperature second-order* constitutive model for diatomic and polyatomic gases with vibrational non-equilibrium can be derived:

$$
\begin{aligned}
2[\mathbf{\Pi}\cdot\nabla\mathbf{u}]^{(2)}+2(p+\Delta)[\nabla\mathbf{u}]^{(2)} &= -\frac{p}{\mu}\mathbf{\Pi}q_{2nd}(\kappa),\\
2\gamma'(\mathbf{\Pi}+\Delta\mathbf{I}):\nabla\mathbf{u}+\frac{2}{3}\gamma' p\nabla\cdot\mathbf{u} &= -\frac{2}{3}\gamma'\frac{p}{\mu_b}\Delta q_{2nd}(\kappa),\\
\mathbf{\Pi}\cdot\nabla(C_pT)+(p+\Delta)\nabla(C_pT) &= -\frac{pC_p}{k}\mathbf{Q}q_{2nd}(\kappa),\\
\mathbf{\Pi}\cdot\nabla(C_{p,v}T_v)+(p+\Delta)\nabla(C_{p,v}T_v) &= -\frac{pC_{p,v}T_v}{k_v}\mathbf{Q}_v q_{2nd}(\kappa).
\end{aligned}
\tag{5}
$$

A detailed description of the derivation of the modified Curtiss-Boltzmann equation and associated NCCR model for diatomic and polyatomic gases can be found in previous work [52].

The exact form of the second-order dissipation $q_{2nd}(\kappa)$ and the cumulant expansion κ can be calculated using the cumulant expansion method and the Chapman-Enskog theory, respectively,

$$
\begin{aligned}
q_{2nd}(\kappa) &= \frac{\sinh(\kappa)}{\kappa},\\
\kappa &= \frac{(mk_B)^{1/4}}{\sqrt{2}d}\frac{T^{1/4}}{p}\left[\frac{\mathbf{\Pi}:\mathbf{\Pi}}{2\mu}+\gamma'\frac{\Delta^2}{\mu_b}+\frac{\mathbf{Q}\cdot\mathbf{Q}/T}{k}+\frac{\mathbf{Q}_v\cdot\mathbf{Q}_v/T_v}{k_v}\right]^{1/2},
\end{aligned}
\tag{6}
$$

where m is the molecule mass, d is the molecular diameter and molecule mass, μ is the viscosity, μ_b is the bulk viscosity, k is the thermal conductivity, and k_v is the vibrational thermal conductivity.

The quadratic form of the cumulant expansion κ is equal to a modified Rayleigh-Onsager dissipation function [55] and is represented by the sum of the double scalar product between

tensors and the dot product of the heat flux vector, which gives a direct measure of departure from equilibrium. The second-order approximation of the dissipation term, " $q_{2nd}(\kappa)$," describes the mode of energy dissipation accompanying the irreversible processes and is directly related to the non-equilibrium entropy production in the system. The subscript "*2nd*" highlights the second-order closure applied to Eqs. (5) and (6). The derivation of the hyperbolic sine function, $q_{2nd}(\kappa)$, can be found in detail in the references [2,22,23,52]. The concept of dissipation functions for irreversible processes was introduced by Onsager in 1931 [55].

The second-order NCCR (5) is reduced to the following conventional first-order NSF constitutive relations, when the first-order approximations, the zero bulk viscosity assumption, $\mu_b = 0$, and the constant $C_p, C_{p,v}$ assumption are employed,

$$
\begin{aligned}
2\,p[\nabla\mathbf{u}]^{(2)} = -\frac{p}{\mu}\boldsymbol{\Pi} \;&\Rightarrow\; \boldsymbol{\Pi} = -2\mu[\nabla\mathbf{u}]^{(2)}, \\
p\nabla\cdot\mathbf{u} = -\frac{p}{\mu_b}\Delta \text{ or } \Delta = -\mu_b(\nabla\cdot\mathbf{u}) \;&\Rightarrow\; \Delta = 0, \\
p\nabla(C_pT) = -\frac{pC_p}{k}\mathbf{Q} \;&\Rightarrow\; \mathbf{Q} = -k\nabla T, \\
p\nabla(C_{p,v}T_v) = -\frac{pC_{p,v}}{k_v}\mathbf{Q}_v \;&\Rightarrow\; \mathbf{Q}_v = -k_v\nabla T_v,
\end{aligned}
\tag{7}
$$

meaning that the NSF is simply a subset of the NCCR. It should be mentioned that these first-order laws were obtained after very crude approximations; all of the kinematic terms except for the thermodynamic force term were neglected, the dissipation terms were linearized with $q_{2nd}(\kappa) = 1$, and $C_p, C_{p,v}$ were assumed constant.

2.2. *NCCR model in the compact dimensionless form*

The second-order constitutive relation in the dimensional form can be transformed into a compact non-dimensional form. The following dimensionless variables and the definitions of non-dimensional parameters (such as the Mach number (*M*), Reynolds number (Re), Eckart number (Ec), Prandtl number (Pr), Knudsen number (Kn), and non-dimensional rarefaction parameter (N_δ)) are employed [52]:

$$t^* = \frac{t}{\left(L/a_r\right)},\quad \boldsymbol{x}^* = \frac{\boldsymbol{x}}{L},\quad \nabla^* = L\nabla,\quad \mu^* = \frac{\mu}{\mu_r},\quad k^* = \frac{k}{k_r},\quad \boldsymbol{u}^* = \frac{\boldsymbol{u}}{u_r},$$

$$p^* = \frac{p}{p_r},\quad \rho^* = \frac{\rho}{\rho_r},\quad T^* = \frac{T}{T_r},\quad C_p^* = \frac{C_p}{C_{p_r}},\quad e^* = \frac{e}{u_r^2},\quad d^* = \frac{d}{d_r},$$

$$\boldsymbol{\Pi}^* = \frac{\boldsymbol{\Pi}}{\left(\mu_r u_r/L\right)},\quad \Delta^* = \frac{\Delta}{\left(\mu_r u_r/L\right)},\quad \mathbf{Q}^* = \frac{\mathbf{Q}}{\left(k_r T_r/L\right)},\quad f_b = \frac{\mu_{b_r}}{\mu_r},$$

$$M = \frac{u_r}{\sqrt{\gamma R T_r}},\quad \mathrm{Re} = \frac{\rho_r u_r L}{\mu_r},\quad \mathrm{Ec} = \frac{u_r^2}{C_{p_r} T_r},\quad \mathrm{Pr} = \frac{c_{p_r}\mu_r}{k_r},\quad \varepsilon = \frac{1}{\mathrm{EcPr}},$$

$$N_\delta = \frac{\gamma M^2}{\mathrm{Re}},\quad \mathrm{Kn} = \sqrt{\frac{\pi}{2\gamma}}\frac{N_\delta}{M}.$$

Here the starred quantities represent the non-dimensional quantities; terms with subscript *r* are reference quantities chosen appropriate to the flow problem. The factor $f_b = \mu_{b_r} / \mu_r$ is the ratio of the bulk viscosity to the shear viscosity. In addition to the above-mentioned non-dimensional entities, an additional set of non-dimensional quantities and parameters are defined for the vibrational degrees of freedom:

$$k_v^* = \frac{k_v}{k_{v,r}},\quad T_v^* = \frac{T_v}{T_{v,r}},\quad C_{p,v}^* = \frac{C_{p,v}}{C_{p,v_r}},\quad e_v^* = \frac{e_v}{u_r^2},\quad \tau_v^* = \frac{\tau_v}{L/u_r},\quad \dot{\omega}_v^* = \frac{\dot{\omega}_v}{\rho_r u_r^2/(L/u_r)},$$

$$\mathbf{Q}_v^* = \frac{\mathbf{Q}_v}{\left(k_{v,r}T_{v,r}/L\right)},\quad \mathrm{Ec}_v = \frac{u_r^2}{C_{p,v_r}T_{v,r}},\quad \mathrm{Pr}_v = \frac{c_{p,v_r}\mu_r}{k_{v,r}},\quad \varepsilon_v = \frac{1}{\mathrm{Ec}_v\mathrm{Pr}_v}. \tag{8}$$

After those non-dimensional quantities and parameters are substituted into the conservation laws (2) and (3), the second-order NCCR model (5), and the modified Rayleigh-Onsager dissipation function (6), and dropping the asterisk superscript for simplicity, the following conservation laws and NCCR model in a compact form can be obtained:

$$\frac{\partial}{\partial t}\begin{bmatrix}\rho\\ \rho\mathbf{u}\\ \rho e\\ \rho e_v\end{bmatrix} + \nabla\cdot\begin{bmatrix}\rho\mathbf{u}\\ \rho\mathbf{u}\mathbf{u} + \dfrac{1}{\gamma M^2}p\mathbf{I}\\ \left(\rho e + \dfrac{1}{\gamma M^2}p\right)\mathbf{u}\\ \rho e_v\mathbf{u}\end{bmatrix} + \frac{1}{\mathrm{Re}}\nabla\cdot\begin{bmatrix}0\\ \boldsymbol{\Pi} + \Delta\mathbf{I}\\ \left(\boldsymbol{\Pi} + \Delta\mathbf{I}\right)\cdot\mathbf{u} + \varepsilon\mathbf{Q} + \varepsilon_v\mathbf{Q}_v\\ \varepsilon_v\mathbf{Q}_v\end{bmatrix} = \begin{bmatrix}0\\ 0\\ 0\\ \dot{\omega}_v\end{bmatrix}, \tag{9}$$

and

$$\begin{aligned}
\hat{\mathbf{\Pi}} q_{2nd}(c\hat{R}) &= (1+\hat{\Delta})\hat{\mathbf{\Pi}}_0 + [\hat{\mathbf{\Pi}}\cdot\nabla\hat{\mathbf{u}}]^{(2)}, \\
\hat{\Delta} q_{2nd}(c\hat{R}) &= \hat{\Delta}_0 + \frac{3}{2} f_b(\hat{\mathbf{\Pi}} + \hat{\Delta}\mathbf{I}) : \nabla\hat{\mathbf{u}}, \\
\hat{\mathbf{Q}} q_{2nd}(c\hat{R}) &= (1+\hat{\Delta})\hat{\mathbf{Q}}_0 + \hat{\mathbf{\Pi}}\cdot\hat{\mathbf{Q}}_0, \\
\hat{\mathbf{Q}}_v q_{2nd}(c\hat{R}) &= (1+\hat{\Delta})\hat{\mathbf{Q}}_{v,0} + \hat{\mathbf{\Pi}}\cdot\hat{\mathbf{Q}}_{v,0},
\end{aligned} \tag{10}$$

where

$$\begin{aligned}
q_{2nd}(c\hat{R}) &= \frac{\sinh(c\hat{R})}{c\hat{R}}, \\
\hat{R} &= \left[\hat{\mathbf{\Pi}} : \hat{\mathbf{\Pi}} + \frac{2\gamma'}{f_b}\hat{\Delta}^2 + \hat{\mathbf{Q}}\cdot\hat{\mathbf{Q}} + \hat{\mathbf{Q}}_v\cdot\hat{\mathbf{Q}}_v \right]^{1/2}.
\end{aligned} \tag{11}$$

In this expression, the coefficient c was first derived by Myong [3] with a simple gas assumption:

$$c \equiv \left(\frac{(mk_B T_r)^{1/4}}{2d_r\sqrt{\mu_r}} \right) = \left[\frac{2\sqrt{\pi}}{5} A_2(\nu)\Gamma[4-2/(\nu-1)] \right]^{1/2},$$

where ν is the exponent of the inverse power laws. The following hat quantities have also been applied:

$$\begin{aligned}
&\hat{\mathbf{\Pi}} \equiv \frac{N_\delta}{p}\mathbf{\Pi}, \quad \hat{\Delta} \equiv \frac{N_\delta}{p}\Delta, \quad \hat{\mathbf{Q}} \equiv \frac{N_\delta}{p}\frac{\mathbf{Q}}{\sqrt{T/(2\varepsilon)}}, \quad \hat{\mathbf{Q}}_v \equiv \frac{N_\delta}{p}\frac{\mathbf{Q}_v}{\sqrt{T_v/(2\varepsilon_v)}}, \\
&\hat{\mathbf{\Pi}}_0 \equiv \frac{N_\delta(-2\mu[\nabla\mathbf{u}]^{(2)})}{p} = [\nabla\hat{\mathbf{u}}]^{(2)}, \quad \hat{\Delta}_0 \equiv \frac{N_\delta(-\mu_b\nabla\cdot\mathbf{u})}{p} = f_b(\nabla\cdot\hat{\mathbf{u}}), \quad , \\
&\hat{\mathbf{Q}}_0 \equiv \frac{N_\delta}{p}\frac{(-k\nabla T)}{\sqrt{T/(2\varepsilon)}} = \nabla\hat{T}, \quad \hat{\mathbf{Q}}_{v,0} \equiv \frac{N_\delta}{p}\frac{(-k_v\nabla T_v)}{\sqrt{T_v/(2\varepsilon_v)}} = \nabla\hat{T}_v.
\end{aligned} \tag{12}$$

On the other hand, it is possible to choose dimensionless variables such that the dimensionless form of inviscid fluxes in the conservation laws is the same as the original dimensional form of inviscid fluxes. This form is very convenient because it does not require any modifications to the various flux functions designed to calculate the inviscid fluxes. When all terms in the conservation laws are normalized using the following variables and parameters,

$$t^* = \frac{t}{\left(L/a_r\right)},\quad \boldsymbol{x}^* = \frac{\boldsymbol{x}}{L},\quad \nabla^* = L\nabla,\quad \mu^* = \frac{\mu}{\mu_r},\quad k^* = \frac{k}{k_r},\quad \boldsymbol{u}^* = \frac{\boldsymbol{u}}{a_r},$$

$$p^* = \frac{p}{\rho_r a_r^2},\quad \rho^* = \frac{\rho}{\rho_r},\quad T^* = \frac{T}{T_r},\quad C_p^* = \frac{C_p}{a_r^2/T_r},\quad e^* = \frac{e}{a_r^2},\quad d^* = \frac{d}{d_r},$$

$$\boldsymbol{\Pi}^* = \frac{\boldsymbol{\Pi}}{\left(\mu_r a_r/L\right)},\quad \Delta^* = \frac{\Delta}{\left(\mu_r a_r/L\right)},\quad \mathbf{Q}^* = \frac{\mathbf{Q}}{\left(k_r T_r/L\right)},\quad f_b = \frac{\mu_{b_r}}{\mu_r},$$

$$M = 1,\ \mathrm{Re} = \frac{\rho_r a_r L}{\mu_r},\ \mathrm{Ec} = \frac{a_r^2}{C_{p_r} T_r},\ \mathrm{Pr} = \frac{c_{p_r}\mu_r}{k_r},\quad \varepsilon = \frac{1}{\mathrm{EcPr}},$$

$$N_\delta = \frac{1}{\mathrm{Re}},\quad \mathrm{Kn} = \sqrt{\frac{\gamma\pi}{2}}\frac{1}{\mathrm{Re}},$$

together with parameters defined for the vibrational degrees of freedom,

$$k_v^* = \frac{k_v}{k_{v,r}},\quad T_v^* = \frac{T_v}{T_{v,r}},\quad C_{p,v}^* = \frac{C_{p,v}}{C_{p,v_r}},\quad e_v^* = \frac{e_v}{a_r^2},\quad \tau_v^* = \frac{\tau_v}{L/a_r},\quad \dot{\omega}_v^* = \frac{\dot{\omega}_v}{\rho_r a_r^2/(L/a_r)},$$

$$\mathbf{Q}_v^* = \frac{\mathbf{Q}_v}{\left(k_{v,r}T_{v,r}/L\right)},\quad \mathrm{Ec}_v = \frac{u_r^2}{C_{p,v_r}T_{v,r}},\quad \mathrm{Pr}_v = \frac{c_{p,v_r}\mu_r}{k_{v,r}},\quad \varepsilon_v = \frac{1}{\mathrm{Ec}_v\mathrm{Pr}_v},$$

(13)

the dimensionless form of inviscid fluxes in the conservation laws remains the same as the original dimensional form.

$$\frac{\partial}{\partial t}\begin{bmatrix}\rho\\ \rho\mathbf{u}\\ \rho e\\ \rho e_v\end{bmatrix} + \nabla\cdot\begin{bmatrix}\rho\mathbf{u}\\ \rho\mathbf{u}\mathbf{u}+p\mathbf{I}\\ (\rho e+p)\mathbf{u}\\ \rho e_v\mathbf{u}\end{bmatrix} + \frac{1}{\mathrm{Re}}\nabla\cdot\begin{bmatrix}0\\ \boldsymbol{\Pi}+\Delta\mathbf{I}\\ (\boldsymbol{\Pi}+\Delta\mathbf{I})\cdot\mathbf{u}+\varepsilon\mathbf{Q}+\varepsilon_v\mathbf{Q}_v\\ \varepsilon_v\mathbf{Q}_v\end{bmatrix} = \begin{bmatrix}0\\ 0\\ 0\\ \dot{\omega}_v\end{bmatrix}, \tag{14}$$

Note that the acoustic speed (a_r), instead of the velocity (u_r), is used in defining the reference value. On the other hand, the corresponding algebraic constitutive relations (10)-(12) remain unchanged.

2.3. *Velocity slip and temperature jump conditions for multi-dimensional simulation*

The velocity slip and temperature jump boundary conditions on the solid surface are necessary to accurately describe rarefied and microscale gas flows [56–58]. In 1879, Maxwell introduced a velocity slip boundary condition known as the Maxwell velocity slip condition [59]. In this boundary condition, the slip in tangential velocity near a solid surface $\mathbf{u}_{\mathrm{slip}}$ is related to the tangential shear stress $\boldsymbol{\Pi}_{\tan}$ and the tangential heat flux $\mathbf{Q}_{\tan}$. This slip condition can be expressed in the following form [58,59],

$$\mathbf{u}_{\text{slip}} - \mathbf{u}_{\text{wall}} = -\left(\frac{2-\sigma_v}{\sigma_v}\right)\frac{\lambda_{\text{mean}}}{\mu}\boldsymbol{\Pi}_{\tan} - \frac{3}{4}\frac{\Pr(\gamma-1)}{\gamma p}\mathbf{Q}_{\tan}, \tag{15}$$

where $\mathbf{u}_{\text{wall}}$ is the velocity vector of a solid surface, and λ_{mean} denotes the mean free path. We assume the solid surface is located at the origin of the normal coordinate. The tangential momentum accommodation coefficient is denoted by $\sigma_v\,(0 \le \sigma_v \le 1)$ which determines the proportion of the molecules reflected from the surface purely diffusely ($\sigma_v = 1$) or purely specular ($\sigma_v = 0$). The tangential shear stress and the tangential heat flux are defined in general coordinates at the surface,

$$\begin{aligned} \boldsymbol{\Pi}_{\tan} &= (\mathbf{n}\cdot\boldsymbol{\Pi})\cdot\mathbf{S}, \\ \mathbf{Q}_{\tan} &= \mathbf{Q}\cdot\mathbf{S}, \end{aligned} \tag{16}$$

where the **S**, defined as $\mathbf{S}=\mathbf{I}-\mathbf{n}\otimes\mathbf{n}$ using the dyadic product ($\otimes$), refers to the surface vector in which normal components are removed. If the constitutive relations of viscous stress and heat flux are taken as linear with first-order accuracy, the slip condition (15) is simplified in cartesian coordinates into

$$u_{\text{slip}} - u_{\text{wall}} = \left(\frac{2-\sigma_v}{\sigma_v}\right)\lambda_{\text{mean}}\frac{\partial u}{\partial y} + \frac{3}{4}\frac{\Pr(\gamma-1)}{\gamma p}k\frac{\partial T}{\partial x}. \tag{17}$$

By analogy with the Maxwell velocity slip condition, the Smoluchowski jump boundary condition [60,58] can be written as

$$T_{\text{slip}} - T_{\text{wall}} = -\left(\frac{2-\sigma_T}{\sigma_T}\right)\frac{\lambda_{\text{mean}}}{k}\frac{2\gamma}{(\gamma+1)\Pr}\mathrm{Q}_{\text{normal}}. \tag{18}$$

Here T_{slip} is the gas temperature at the surface, T_{wall} is the temperature of the solid surface, and $\sigma_T\,(0 \le \sigma_T \le 1)$ denotes the thermal accommodation coefficient. If the constitutive relation of heat flux is taken as linear with first-order accuracy, the jump condition (18) is simplified in cartesian coordinates into

$$T_{\text{slip}} - T_{\text{wall}} = \left(\frac{2-\sigma_T}{\sigma_T}\right)\lambda_{\text{mean}}\frac{2\gamma}{(\gamma+1)\Pr}\frac{\partial T}{\partial y}. \tag{19}$$

3. Methodologies for solving NCCR

The strategy to numerically solve the conservation laws in conjunction with NCCR has two main issues. The first issue is the choice of the computational methodology to handle the conservation laws with various options such as the finite volume method (FVM), finite element method (FEM), spectral methods, and continuous and discontinuous Galerkin (DG) methods. For example, our group developed in-house codes based on FVM and a mixed modal DG method [39–43].

The second issue is how to solve NCCR, (10)-(12), to determine the non-conserved quantities—viscous stress, excess normal stress, heat flux, and vibrational heat flux—for given thermodynamic forces (gradients of velocity, trans-rotational and vibrational temperatures). The first-order NSF calculations are straightforward since these quantities are proportional to gradients of velocity and temperatures. In contrast, since the second-order NCCR is nonlinear and highly coupled, an appropriate numerical strategy must be developed. Moreover, the NCCR of viscous shear stress is in the form of a second-rank tensorial equation, which is particularly complex to solve in 2D and 3D flow simulations. The viscous shear stress tensor is traceless and hence contains only 5 independent elements ($\hat{\Pi}_{11}$, $\hat{\Pi}_{12}$, $\hat{\Pi}_{13}$, $\hat{\Pi}_{22}$, $\hat{\Pi}_{23}$, $-\hat{\Pi}_{11}-\hat{\Pi}_{22}$). Thus, along with the excess normal stress $\hat{\Delta}$ and 6 components of the two heat flux vectors ($\hat{Q}_1$, $\hat{Q}_2$, $\hat{Q}_3$) and ($\hat{Q}_{v,1}$, $\hat{Q}_{v,2}$, $\hat{Q}_{v,3}$), a total of 12 unknowns have to be calculated from the given 17 known variables ($p, T, \nabla\mathbf{u}, \nabla T, \nabla T_v$).

3.1. *Method I: Iterative method based on decomposition at the cell interface*

One way to drastically reduce the complexity of solving 12 equations is to apply NCCR to the interface (or edge) of a computational cell, rather than a node. The 3D flow problem can then be split into three sub-problems in the x, y, z directions in any computational framework. Further, the viscous stress and heat flux components ($\hat{\Pi}_{11}$, $\hat{\Pi}_{12}$, $\hat{\Pi}_{13}$, $\hat{\Delta}$, $\hat{Q}_1$, $\hat{Q}_{v,1}$) on a surface in a three-dimensional control volume induced by thermodynamic driving forces (gradients of velocity and temperatures) can be approximated as the sum of three decomposed solvers; first on ($\partial u_1/\partial x_1$, 0, 0, $\partial T/\partial x_1$, $\partial T_v/\partial x_1$) describing the compression-expansion flow, second on (0, $\partial u_2/\partial x_1$, 0, 0, 0), and third on (0, 0, $\partial u_3/\partial x_1$, 0, 0) describing the velocity-shear flow, that is,

$$f(\hat{\Pi}_{11},\hat{\Pi}_{12},\hat{\Pi}_{13},\hat{\Delta},\hat{Q}_1,\hat{Q}_{v,1}) = f_1(\partial u_1/\partial x_1, 0, 0, \partial T/\partial x_1, \partial T_v/\partial x_1) + f_2(0, \partial u_2/\partial x_1, 0, 0, 0) + f_3(0, 0, \partial u_3/\partial x_1, 0, 0) \quad (20)$$

Note that the decomposition of these viscous fluxes has the same spirit as the treatment of inviscid fluxes: $F(\rho u_1, \rho u_1 u_1 + p, \rho u_1 u_2, \rho u_1 u_3, (\rho e + p)u_1, \rho e_v u_1) = F_1(\rho u_1, \rho u_1 u_1 + p, 0, 0, (\rho e + p)u_1, \rho e_v u_1) + F_2(0, 0, \rho u_1 u_2, 0, 0, 0) + F_2(0, 0, 0, \rho u_1 u_3, 0, 0)$.

The iterative procedure can be developed individually for the decomposed solvers. For a sub-domain determined by the sign of the first-order NSF constitutive laws based on gradients of velocity and temperatures, it is possible to find iterative functions that always converge over the whole sub-domain. Similarly, it is possible to solve the decomposed solvers along the *y*- and *z*-direction, and the component-wise values are summed up to obtain the final results. In the case of the steady-state problem, it was observed that the convergence can be improved by first solving the entire problem using the first-order NSF constitutive laws and then employing the NCCR model with the NSF quantities as the initial condition. A detailed description of method I in multi-dimensional flow problems is given in previous works [4,42].

3.2. *Method II: Undecomposed relaxation method*

In the present work, an alternative iterative scheme is presented. The broader objective of this work is to implement the NCCR theory in the *foam-extend* based *dbnsTurbFoam* solver. The *foam-extend* is a variant of the *OpenFOAM* (Open-source Field Operation and Manipulation) C++ toolbox for CFD. A prime advantage of this toolkit is the efficiency of tensor algebra programming. This aspect of the OpenFOAM toolbox inspires method II. However, this strategy can be implemented in conventional FVM and DG in-house codes as well. Method I begins with calculating the inviscid fluxes, initializing viscous stresses and heat fluxes as the first-order approximations, calculating the second-order viscous stresses and heat fluxes using iterative schemes, and finally merging the second-order viscous fluxes to calculate the conserved quantities at the next time-step using a standard time-integrator.

The procedure of the new alternative scheme does not involve solving the second-order NCCR iteratively until convergence in each time step. The tensor equations are not decomposed into a set of component-wise equations in this method. Instead, the tensorial and vectorial equations for calculating the viscous stresses and heat fluxes, respectively, are solved directly. The nonlinear coupled algebraic equations are generally difficult to solve using

analytical methods or using single-step numerical procedures. However, an iterative scheme with appropriate under-relaxation can solve the equation without much difficulty.

To illustrate the essence of method II, consider an isothermal monoatomic gas simulation. In this case, the second-order NCCR of viscous stresses is nonlinear and coupled, but not related to heat flux. The viscous stress tensor appears at three different places in the implicit NCCR. To solve the NCCR in its native tensorial form, the viscous stress term multiplied by the nonlinear term $q_{2nd}(c\hat{R})$ is chosen as the primary unknown, and the value of viscous stress in the remaining two places is taken from the previous iteration. The tensor equation can then be directly solved using the following iterative procedure:

$$\hat{\mathbf{\Pi}}^{n+1} = \alpha\hat{\mathbf{\Pi}}^{n} + (1-\alpha)\frac{(\hat{\mathbf{\Pi}}_0 + [\hat{\mathbf{\Pi}}^{n}\cdot\nabla\hat{\mathbf{u}}]^{(2)})}{q_{2nd}(c\sqrt{\hat{\mathbf{\Pi}}^{n}:\hat{\mathbf{\Pi}}^{n}})}, \tag{21}$$

where α is the under-relaxation parameter. The quantities with zero as a subscript represent the first-order NSF approximation. Convergence for this second-rank tensorial equation is assured for values of the under-relaxation parameter less than 0.1. Such a low value of the under-relaxation parameter indicates the highly nonlinear nature of the equation, which is highlighted by the presence of the hyperbolic sine term.

In this study, instead of solving the NCCR iteratively till convergence in each evolution step, the computation is performed only once per computational cell. In this manner, the conserved and non-conserved variables converge simultaneously. In other words, the present code avoids a situation of a nested loop where the outer loop is for the evolution of the conserved variables along the time direction, and the inner loop is for the iterative method for calculating the second-order non-conserved variables. However, since the degree of nonlinearity increases with the coupled nature of the second-order non-conserved variables, the suggested value of the permissible under-relaxation reduces to 0.01. The final under-relaxed set in the case of monoatomic gases is

$$\begin{aligned}
\hat{\mathbf{\Pi}}^{n+1} &= \alpha\hat{\mathbf{\Pi}}^{n} + (1-\alpha)\frac{(\hat{\mathbf{\Pi}}_0 + [\hat{\mathbf{\Pi}}^{n}\cdot\nabla\hat{\mathbf{u}}]^{(2)})}{q_{2nd}(c\sqrt{\hat{\mathbf{\Pi}}^{n}:\hat{\mathbf{\Pi}}^{n} + \hat{\mathbf{Q}}^{n}\cdot\hat{\mathbf{Q}}^{n}})}, \\
\hat{\mathbf{Q}}^{n+1} &= \alpha\hat{\mathbf{Q}}^{n} + (1-\alpha)\frac{\hat{\mathbf{Q}}_0 + \hat{\mathbf{\Pi}}^{n}\cdot\hat{\mathbf{Q}}_0}{q_{2nd}(c\sqrt{\hat{\mathbf{\Pi}}^{n}:\hat{\mathbf{\Pi}}^{n} + \hat{\mathbf{Q}}^{n}\cdot\hat{\mathbf{Q}}^{n}})}.
\end{aligned} \tag{22}$$

In the case of diatomic and polyatomic gases with vibrational non-equilibrium, the equations (10)-(12) in the two-temperature framework provide a total of four systems as follows,

$$\hat{\mathbf{\Pi}}^{n+1} = \alpha\hat{\mathbf{\Pi}}^{n} + (1-\alpha)\frac{(1+\hat{\Delta}^{n})\hat{\mathbf{\Pi}}_{0} + [\hat{\mathbf{\Pi}}^{n}\cdot\nabla\hat{\mathbf{u}}]^{(2)}}{q_{2nd}(c\sqrt{\hat{\mathbf{\Pi}}^{n}:\hat{\mathbf{\Pi}}^{n} + 2\gamma'(\hat{\Delta}^{n})^{2}/\ f_{b} + \hat{\mathbf{Q}}^{n}\cdot\hat{\mathbf{Q}}^{n} + \hat{\mathbf{Q}}_{v}^{n}\cdot\hat{\mathbf{Q}}_{v}^{n}})},$$

$$\hat{\Delta}^{n+1} = \alpha\hat{\Delta}^{n} + (1-\alpha)\frac{\hat{\Delta}_{0} + 3f_{b}(\hat{\mathbf{\Pi}}^{n} + \hat{\Delta}^{n}\mathbf{I}):\nabla\hat{\mathbf{u}}/2}{q_{2nd}(c\sqrt{\hat{\mathbf{\Pi}}^{n}:\hat{\mathbf{\Pi}}^{n} + 2\gamma'(\hat{\Delta}^{n})^{2}/\ f_{b} + \hat{\mathbf{Q}}^{n}\cdot\hat{\mathbf{Q}}^{n} + \hat{\mathbf{Q}}_{v}^{n}\cdot\hat{\mathbf{Q}}_{v}^{n}})},$$

$$\hat{\mathbf{Q}}^{n+1} = \alpha\hat{\mathbf{Q}}^{n} + (1-\alpha)\frac{(1+\hat{\Delta}^{n})\hat{\mathbf{Q}}_{0} + \hat{\mathbf{\Pi}}^{n}\cdot\hat{\mathbf{Q}}_{0}}{q_{2nd}(c\sqrt{\hat{\mathbf{\Pi}}^{n}:\hat{\mathbf{\Pi}}^{n} + 2\gamma'(\hat{\Delta}^{n})^{2}/\ f_{b} + \hat{\mathbf{Q}}^{n}\cdot\hat{\mathbf{Q}}^{n} + \hat{\mathbf{Q}}_{v}^{n}\cdot\hat{\mathbf{Q}}_{v}^{n}})},$$

$$\hat{\mathbf{Q}}_{v}^{n+1} = \alpha\hat{\mathbf{Q}}_{v}^{n} + (1-\alpha)\frac{(1+\hat{\Delta}^{n})\hat{\mathbf{Q}}_{v,0} + \hat{\mathbf{\Pi}}^{n}\cdot\hat{\mathbf{Q}}_{v,0}}{q_{2nd}(c\sqrt{\hat{\mathbf{\Pi}}^{n}:\hat{\mathbf{\Pi}}^{n} + 2\gamma'(\hat{\Delta}^{n})^{2}/\ f_{b} + \hat{\mathbf{Q}}^{n}\cdot\hat{\mathbf{Q}}^{n} + \hat{\mathbf{Q}}_{v}^{n}\cdot\hat{\mathbf{Q}}_{v}^{n}})}. \tag{23}$$

Method II can make use of *OpenFOAM* which has a pre-defined library of tensor algebra operations. The choice of under-relaxation parameter turns out to be critical to the stability of the simulation. It was observed that in the case of very rare situations such as gases with very high bulk viscosity (f_b □ 1), the under-relaxation was an order of magnitude smaller than the one recommended earlier, which slows down convergence. Method I does not employ any such under-relaxation parameter and has been proven to lead to convergence in almost all scenarios.

4. Development of *nccrFOAM* code

4.1. *Introduction to dbnsFoam and dbnsTurbFoam*

The *rhoCentralFoam* solver [61] is the most widely used density-based solver for compressible flow that comes pre-installed with the official *OpenFOAM* distribution. This solver employs the Kurganov and Tadmor (KT) [62], and Kurganov, Noelle, and Tadmor(KNP) [63] flux schemes for handling the nonlinear terms in the Euler/NSF equations. KT and KNP flux schemes avoid expensive Jacobian evaluations as they use a central difference-based formulation instead of solving the Riemann problem for flux calculation. However, it has been observed that the shock structures computed using the central difference schemes are prone to dissipative effects. Recently, improved density-based solvers named *dbnsFOAM* and *dbnsTurbFOAM* solvers have been developed and included in the *foam-extend* framework, which is another fork of *OpenFOAM*. The two density-based solvers employ the *dbns* or density-based Navier-Stokes library.

Several options are available for time-integrators in the *foam-extend* framework and can be employed to track the evolution of the conserved variables over time. The central problem

when solving the nonlinear system of conservation laws, such as the Euler equation or the Navier-Stokes-Fourier equation is the calculation of the flux terms at the cell interfaces. *nccrFOAM* employs approximate Riemann solvers [64] to calculate the numerical approximation of the flux at the interfaces. The *dbns* library contains several state-of-the-art approximate Riemann solvers such as the HLLC (Harten-Lax-vanLeer+Contact) family of solvers [65,66], Roe approximate Riemann solver [67], Rusanov flux [68] schemes, and AUSM (Advection Upstream Splitting Method) family of flux vector splitting schemes [68, 69]. The *dbnsFOAM* and *dbnsTurbFOAM* solvers also have higher-order reconstruction schemes and a wide range of options for slope limiters.

4.2. *nccrFOAM suite file structure*

The new *nccrFOAM* suite is derived from the *dbnsTurbFOAM* solver that employs the *dbns* library in a *foam-extend* fork of the *OpenFOAM* framework. Overall, the development of the *nccrFOAM* suite is divided into two parts:

- *nccrFOAM*: adding the second-order NCCR for monoatomic, diatomic, and polyatomic gases at a lower temperature in the absence of vibrational non-equilibrium,
- *nccrVibFOAM*: adding the two-temperature formulation to the NSF solver for handling non-equilibrium flows, and further adding the NCCR for diatomic and polyatomic gases at higher temperatures with vibrational non-equilibrium.

The first part of the suite requires initializing new variables for the non-conserved quantities (viscous stress tensor and heat flux vector for monoatomic gases, and viscous stress tensor, excess normal stress scalar, and heat flux vector for diatomic and polyatomic gases at lower temperatures) and adding the appropriate equations for the non-conserved quantities to the momentum and energy equations in the algorithm. This will be discussed in the next sub-section in detail.

The second part of the suite requires the manipulation of the *foam-extend* source code at a deeper level, which demands a clear understanding of the *dbns* library. The *dbns* consists of a *basicNumericFlux* class which is a base class for run-time selectable numerical flux methods. In the *creatFields.H* file of a *dbns*-derived solver, an object for numerical flux is initialized using the *New()* function belonging to the *basicNumericFlux* which takes pressure, velocity, and temperature as input. The main class for flux calculation in the *dbns* library is the *numericFlux* class, which is included in the *dbnsFOAM* and *dbnsTurbFOAM* solvers in the header section. The member functions of the *numericFlux* class consist of the following:

• *computeFlux()*: calls the limiter functions and calculates the higher-order reconstruction values for pressure, velocity, and temperatures for a Riemann problem

• *rhoFlux()*: takes the reconstructed Riemann problem initial conditions and returns the flux for the continuity equation by solving the input flux schemes

• *rhoUFlux()*: returns the flux for the momentum equation

• *rhoEFlux()*: returns the flux for the energy equation

The *dbnsFOAM* and *dbnsTurbFOAM* solvers call these functions when solving the three conservation laws. The inclusion of vibrational non-equilibrium in the flow requires adding the vibrational energy equation. A new variable, vibrational energy (*_ev*), also needs to be appended to the conserved variable vector ***U***, which takes the following updated form: $\boldsymbol{U} = [\,\rho\,, \rho\mathbf{u}\,, \rho e\,,\ \rho e_v\,]^{\mathrm{T}}$. The corresponding flux function is $\boldsymbol{F} = [\,\rho\mathbf{u}\,, \rho\mathbf{u}\mathbf{u} + p\mathbf{I}\,, (\rho e + p)\mathbf{u}\ ,\ \rho e_v\mathbf{u}\,]^{T}$ where the last entry is the flux term for the vibrational energy equation. The *dbns* library does not contain a function for calculating flux for the vibrational energy equation and does not take the vibrational temperature as an additional input. The vibrational temperature needs to be added to the modified *New()* function belonging to the *basicNumericFlux* class to provide the necessary variables for calculating the vibrational heat flux. The non-equilibrium modeling requires writing a new *dbns* library based on the existing *dbns* library and contains updated flux functions. Sub-section 4.4 details the new *dbnsv* library that is added to the existing framework to implement the NSF and the NCCR theory for diatomic and polyatomic gas flows with vibrational non-equilibrium.

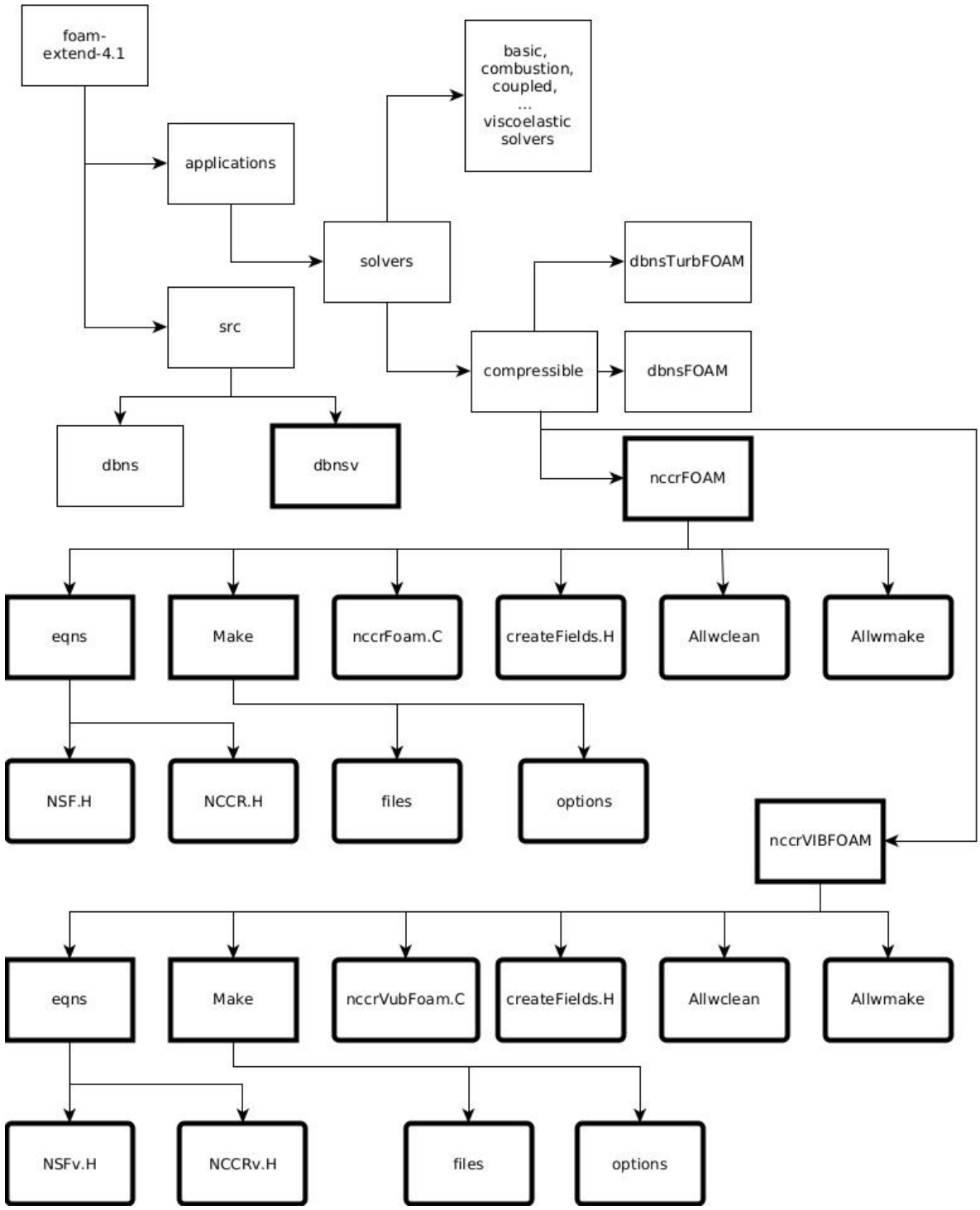

Fig. 1. The file structure of the new *nccrFOAM* and *nccrVibFOAM* solver (Key: rectangle → folders, rounder rectangle → files, darkened icons for newly written files/folders).

The overall file structure of the new solvers in the existing *foam-extend* framework is shown in Fig. 1. The *nccrFOAM* folder consists of the make files along with the source code in *nccrFoam.C*. Similarly, the *nccrVibFOAM* folder containing *nccrVibFoam.C* handles the two-temperature implementation with vibrational non-equilibrium. Depending on the choice of gas system (monoatomic, diatomic, polyatomic, vibrational equilibrium and non-

equilibrium) and the order of the constitutive relations for the non-conserved variables, a suitable system of equations is solved that is stored in the *Eqns* folder and called using a conditional statement from the main source codes (*nccrFOAM.C* or *nccrVibFOAM.C*) of the solver. In the case of *nccrFOAM*, the *Eqns* folder contains the following codes:

- *NSF.H*: solves the Navier-Stokes-Fourier and Navier-Fourier ($f_b > 0$) system of equations to simulate monoatomic, diatomic, and polyatomic gas flows at low temperatures. The code solves the three conservation laws, and the non-conserved variables (viscous shear stress tensor, excess normal stress, and heat flux vector) are calculated using the first-order constitutive laws. This file contains the same code as the *dbnsTurbFoam* main loop.
- *NCCR.H*: solves the nonlinear-coupled constitutive relations (NCCR) to simulate monoatomic, diatomic, and polyatomic gas flows at lower temperatures. The code solves the three conservation laws in conjunction with the second-order NCCR.

Similarly, in the case of *nccrVibFOAM*, the E*qns* folder contains the following codes:

- *NSFv.H*: solves the Navier-Stokes-Fourier and Navier-Fourier ($f_b > 0$) system of equations to simulate diatomic and polyatomic gas flows at high temperatures with vibrational non-equilibrium. The code solves the three conservation laws and an additional equation for vibrational energy. The non-conserved variables (viscous shear stress tensor, excess normal stress, heat flux vector, and vibrational heat flux vector) are calculated using the first-order constitutive laws. The source term in the vibrational energy equation can be modeled using the constant collision factor model, MW, or MWP VT relaxation models.
- *NCCRv.H*: solves the nonlinear-coupled constitutive relations (NCCR) to simulate diatomic and polyatomic gas flows at high temperatures with vibrational non-equilibrium. The code solves the three conservation laws and the fourth vibrational energy equation. The code implements a procedure for solving the second-order NCCR of non-conserved variables (viscous shear stress tensor, excess normal stress, heat flux vector, and vibrational heat flux vector). The source term in the vibrational energy equation is handled in the same manner as in the *NSFv.H* file.

In both solvers, the *createFields.H* contains the details of the variables that are required for the solver. New variables required for solving the equations are added to the existing list of variables. Instead of adding the *dbns* libraries to the main *nccrFoam.C* code, the *dbnsv* has to be added to the header section of the *nccrVibFOAM* solver. The *NSF.H* and *NCCR.H* codes employ/update flux functions from the dbns library, while the *NSFv.H* and *NCCRv.H* codes

employ flux functions from the new dbnsv library, which includes flux functions for the vibrational energy equation.

4.3. Second-order NCCR for monoatomic and low-temperature diatomic and polyatomic gas flows

The first part of the code development is to implement the second-order NCCR for monoatomic and low-temperature diatomic and polyatomic gas flows, which make the *nccrFOAM* solver. A new *IOdictionary* class reference derived from the *dictionary* named *atomProperties* and *IObject* are initialized in the *createFields.H* file as

```
IOdictionary atomProperties
(
      IOobject
      (
            "atomProperties",
            runTime.constant(),
            mesh,
            IOobject::MUST_READ,
      IOobject::NO_WRITE
      )
);
```

This class reference takes the file of the same name residing in the *constant* folder of the simulation folder. Users have to store the values of the Prandtl number (Pr), a reference value of the viscosity coefficient (`muref`) at the specified temperature (`Tref`), index (`omega`) of the power law for calculating viscosity as a function of temperature and specific heat capacity at constant pressure (`Cp`). Further, information on the atomic/molecular mass of the gas (`mass`), atomic/molecular diameter (`diaatom`), the ratio of bulk viscosity to shear viscosity (`fb`), and reference values for velocity (`uRef`), pressure (`pRef`), temperature (`TRef`) and length (`lRef`) are to be specified in the *atomProperties* file when designing the *OpenFOAM* simulation case. Moreover, the users have to add the values for the logical variables for the choice of the order of constitutive relations (`nccr` =0 for the first-order constitutive laws and = 1 for the second-order NCCR). The corresponding variables for these parameters with appropriate dimensions are initialized in the *createFields.H* file, which will search for cases in the *atomProperties* file in the simulation folder at the time of running the case. In the *nccrFOAM*, new volume field variables (`Pi`) (a tensorial variable), (`Delta`) (a scalar variable when $f_b > 0$), and (`Q`) (a vectorial variable) are initialized in the *createFields.H* file.

The *NSF.h* code is simply the *dbnsTurbFOAM* source code with the addition of the power-law for the viscosity coefficient, and for expressing the viscous stress components of the conservation laws in terms of the newly defined volume variables. In the case of the second-order NCCR, the non-conserved variables (viscous shear stress, excess normal stress when $f_b > 0$, and heat flux) are initialized with the first-order approximations in the *nccrFOAM.C* before the main time integrator loop starts. The values of the non-conserved variables will improve with the evolution of the system and eventually converge to accurate second-order approximations. The code for the time integrator loop for the second-order NCCR is written in a separate *C* + + file (*NCCR.H*) in the *Eqns* folder. Solving the second-order NCCR for viscous stress and heat flux for monoatomic gas flows consists of the following steps:

1. Non-dimensionalizing the non-conserved variables: The second-order NCCR can be written in a compact non-dimensional form. The non-dimensional NCCR calculates second-order approximations of the non-dimensional non-conserved variables (`PiND` and `QND`) as a function of non-dimensional first-order thermodynamic forces (`PiNSND` and `QNSND`). Further, the new non-dimensional parameters `cPi` and `cQ` are defined in the createFields.H file.

```
   // Initialize Pi and Q from NSF
volScalarField muEff("muEff", muref*(pow(T/Tref,omega)));
volScalarField kappaEff("kappaEff", muEff*Cp/Pr);
// NSF Stress and Heat Flux
volTensorField tauMC("tauMC", muEff*dev2(Foam::T(fvc::grad(U))));
volTensorField PiNS("PiNS", -(tauMC+ muEff*fvc::grad(U)));
volScalarField DeltaNS("DeltaNS", -(fb*muEff*fvc::div(U)));
volVectorField QNS("QNS", -(fvc::grad(kappaEff*T) - T*fvc ::
grad(kappaEff)));

   // Non-dimensional Stress, Excess stress and Heat Flux
volTensorField PiND("PiND", cPi*Pi/p);
volTensorField PiNSND("PiNSND", cPi*PiNS/p);

volScalarField DeltaND("DeltaND", cPi*Delta/p);
volScalarField DeltaNSND("DeltaNSND", cPi*DeltaNS/p);
volTensorField gradUND("gradUND", -muEff*fvc::grad(U)/p);

volVectorField QND("QND", cQ*Q/p/pow(T,0.5));
volVectorField QNSND("QNSND", cQ*QNS/p/pow(T,0.5));
```

2. Solving the NCCR: The non-dimensional Rayleigh-Onsager dissipation function is calculated, and the second-order NCCR of viscous stress and heat flux are solved using the solve function before the momentum equation. Since these relations are standard algebraic relations, the implementation is straightforward. The snippet of the code is provided here:

```
volScalarField RayOns("RayOns", pow(((PiND&&PiND) + (QND&QND)),0.5));
if(fb.value()>0){
     volScalarField RayOns("RayOns", pow(((PiND && PiND) +
     0.8*DeltaND*DeltaND/fb + (QND & QND)),0.5));
}
    // Solve stress equation
volTensorField p1("p1", PiNSND);
volTensorField p2("p2", PiNSND & (PiND + fb*DeltaND*I2));
volScalarField p3("p3", sinh(c*RayOns+SMALL)/(c*RayOns+SMALL));
PiND =((99.0*PiND)+ (p1+p2)/p3)/100.0;

   // Solve excess stress equation if fb > 0
if(fb.value()>0){
     volScalarField d1("d1", DeltaNSND);
     volScalarField d2("d2", 1.5*fb*((PiND + fb*DeltaND*I2)
     &&(gradUND)));
     volScalarField d3("d3", sinh(c*RayOns+SMALL)/(c*RayOns+SMALL));
     DeltaND =((99.0*DeltaND)+ (d1+d2)/d3)/100.0;
   }

   // Solve heat flux equation
volVectorField q1("q1", QNSND*(1.0+fb*DeltaND));
volVectorField q2("q2", QNSND & PiND);
volScalarField q3("q3", sinh(c*RayOns+SMALL)/(c*RayOns+SMALL));
QND =((99.0*QND)+ (q1+q2)/q3)/100.0;
```

3. Recovering the dimensional non-conserved variables: After solving the non-dimensional equations, the non-dimensional non-conserved variables are transformed back to the dimensional form.

```
// Dimensional Stress and Heat Flux
Pi = p*PiND/cPi;
Delta = p*DeltaND/cPi;
Q = p*pow(T,0.5)*QND/cQ;
```

To simulate diatomic and polyatomic gas flows at low temperatures with bulk viscosity, additional variables for excess normal stress are defined in the *createFields.H* file, and an additional equation of the excess normal stress is added to the *NCCR.H* file. Also, the viscous

stress tensor equation and the heat flux vector equation require minor modifications to incorporate the effect of bulk viscosity. The original *dbnsTurbFoam* density-based compressible solver is suitable for Stokesian fluids. Hence, a new *NSF.H* code is added to the *nccrFOAM* solver, which has an extra capability for simulating flows with non-zero bulk viscosity. The non-conserved variables are calculated using the first-order constitutive laws. The literature on the second-order NCCR generally employs a power law for calculating the viscosity coefficient [2,3]. The power-law model was implemented in the present solver to validate the results of the new solver using those provided in the previous study.

4.4. Second-order NCCR for high-temperature diatomic and polyatomic gas flows with vibrational heat flux

The second solver in the suite, *nccrVibFOAM*, solves diatomic and polyatomic gas flows at high temperatures with vibrational non-equilibrium. The *atomProperties* has additional parameters for VT relaxation models. The *atomProperties* contains the new parameters: the `Zv` constant VT relaxation parameter, `A` and `B` parameters for the MW relaxation model, and constant `sigma` for Park's correction to the MW model, which will be referred to as the MWP relaxation model. If the `Zv` is set to zero, the MW/MWP models will be called to model the V-T relaxation times; otherwise, the constant relaxation model will be employed. When implementing the *nccrVibFOAM* solver, the existing *dbns* library in the *foam-extend* framework is extended to a new library *dbnsv*. The file structure of the *dbnsv* library is shown in Fig. 2.

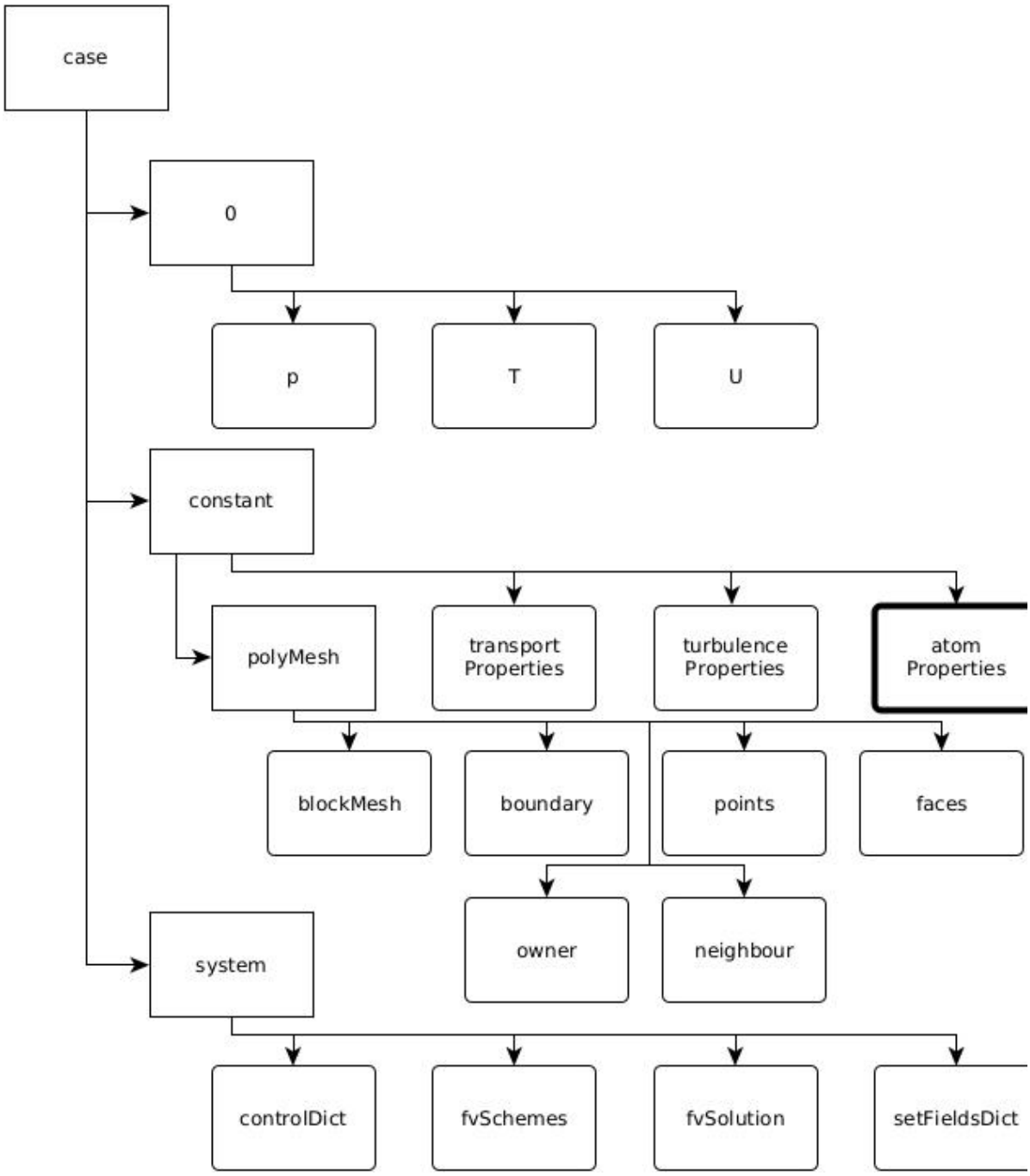

Fig. 2. The file structure of the new *dbnsv* library for two-temperature formulation (Key: rectangle → folders, rounder rectangle → files, darkened icons for newly written files/folders).

As mentioned in the introduction of this section, the vibrational temperature has to be appended to the list of variables in the basicNumericFlux class and its functions by modifying *newBasicNumericFlux.C* in the *basicNumericFlux* folder of the *dbnsv* library. The vibrational energy is calculated using the vibrational temperature (`Tv`), characteristic vibrational temperature (`thetav`), and gas constant (`Rgas`). These scalar variables are also added to the

list of variables in the modified *New()* function. In addition, `rhoEvFlux` in the template of the flux class in the *numericFlux.C* in the *numericFlux* folder is defined in the following manner:

```
rhoEvFlux_
(
    IOobject
    (
        "rhoEvFlux",
        this->mesh().time().timeName(),
        this->mesh(),
        IOobject::NO_READ,
        IOobject::NO_WRITE
    ),
    rhoFlux_*linearInterpolate(Rgas_*thetav_/(exp(thetav_/Tv_) - 1.0))
)
```

The updated *computeFlux()* reconstructs the vibrational temperature and calls the selected flux scheme for the four equations, including the vibrational energy. The flux schemes are located in the *dbnsFlux* folder, and they have to be updated to calculate the additional flux term for the vibrational energy equation. The reconstructed values of pressure, velocity, trans-rotational temperature, and vibrational temperature are input to these flux functions, and they return the flux function values for the four equations. The files related to the reconstruction and limiters are left unchanged. Additional *make* and *include* files are modified to reflect the changes made in the new library. *NSFv.H* and *NCCRv.H* files in the *nccrVibFOAM* solver contain the source code for solving the two-temperature conservation laws with first-order and second-order constitutive relations, respectively.

The overall approach for solving the constitutive relations in *nccrVibFOAM* is similar to that in *nccrFOAM*, by adding the calculation of the vibrational relaxation time and the source term in the vibrational energy equation. The solver in the current form models vibrational relaxation time by either employing the constant VT relaxation model or the MWP model. The parameters required for the two models are defined in the *createFields.H* file. The snippet of code to implement the constant VT relaxation factor model along with the Landau-Teller source term in the vibrational energy equation is as follows,

```
if(Zv.value()>0) {
      // constant VT Model if Zv is initialized in the atomProperties file
   tauZV = Zv*1.25331413732*muEff/(rho*pow(Rgas*T,0.5))/
   (pow(8.0*Rgas*T/3.14159265359,0.5));
}
else {
      // MW and MWP models

   tauZV = constZv*exp(A/pow(T,1.0/3.0)+B)/p +
   1.0/(pow(8.0*Rgas*T/3.14159265359, 0.5)*sigma*rho/mass);

}
      // Solve Vibrational Energy Equation
Solve
(
      1.0/beta[i]*fvm::ddt(rhoEv)
      + fvc::div(dbnsvFlux.rhoEvFlux())
      + fvc::div(Qv)
      - (rho*(Rgas*thetav)/(exp(thetav/T)-1.0) -
      rho*(Rgas*thetav)/(exp(thetav/Tv)-1.0))/tauZV
);
```

where `Zv` is the VT model parameter, *dbnsv.rhoEvFlux()* is the new flux function defined in the *dbnsv* library, and Qv is the vibrational heat flux. `Qv` is a new volume vector appropriately initialized and defined in the *createFields.H* file and is calculated by either the first-order approximation or the second-order NCCR.

5. Verification and validation of *nccrFoam*

Proper verification and validation of the *nccrFOAM* are essential, to assess the accuracy and the robustness of the new solver. *nccrFOAM* solvers are validated using the following two procedures. The first set of simulations reproduces solutions of the second-order NCCR in a simple 1D subset problem. The results calculated by the *nccrFOAM* solvers are compared with those in previous publications [3,4,52]. The present *nccrFOAM* codes are temporarily modified for this test. The time-dependent conservation laws are not solved and only the second-order NCCR is solved by using method II.

Once the veracity of the *nccrFOAM* code is demonstrated, the next set of simulations solves flow problems using the new *nccrFOAM* solvers, where the second-order non-equilibrium effects are prominent and have practical consequences. In the present validation study, we considered several flow problems: 1) a shock structure problem with no vibrational non-equilibrium at Mach 10; 2) a shock structure problem with vibrational non-equilibrium at Mach 15; 3) a hypersonic rarefied gas flow past a cylinder with/without vibrational non-equilibrium;

4) a Poiseuille flow of compressible argon gas through a micro-channel; and 5) a 3D nozzle jet gas impinging onto a surface at near-vacuum. The results were compared with available data such as previous FVM and DSMC results.

5.1 1D simulations and topographical aspects of NCCR

Th one-dimensional NCCR of viscous normal stress arising in the compression-expansion flow problem for a monoatomic gas such as argon, without heat flux, is the simplest yet still powerful validation case. This one-dimensional equation, first derived by Myong in 1999 [3], provides the non-dimensional second-order viscous normal stress as a function of the non-dimensional first-order viscous normal stress defined by NS constitutive laws, highlighting the second-order nonlinear effects of NCCR on the viscous normal stress. The viscous normal stress equation is solved for different cases of initial values. In the *nccrFOAM* framework, this can be calculated by simulating several single-cell domains with $\partial u / \partial x$ as an input. However, in the present case, a single one-dimensional domain is solved to obtain the NCCR stress ($\hat{\Pi}_{xx}$). The *x*-component of the velocity vector in the cells is initialized in such a manner that the non-dimensional NS normal stress along the 1D domain is equal to that showcased on the *x*-axis in Fig. 3a. The flow is assumed to be frozen and the conservation laws in the *nccrFOAM* solver are not solved.

Fig. 3a shows a comparison of the second-order non-dimensional normal stress calculated by the *nccrFOAM* solver and those obtained using the method of iteration reported in the previous literature [3]. The *x*-axis in Fig. 3a represents non-dimensional NS normal stress, which serves as an input. The results of the *nccrFOAM* solver match perfectly with the previous results. Fig. 3a also highlights the difference in the values of normal stress calculated using first- and second-order constitutive relations. In continuum regimes ($\left|\hat{\Pi}_{NS}\right| \ll 1$), the difference between the first-order NS and second-order NCCR results is negligible, justifying the use of NS constitutive relations for most practical flow conditions. However, in highly rarefied regimes, the difference increases in a complex way, especially in the region of gas compression, which corresponds to a positive *x*-axis.

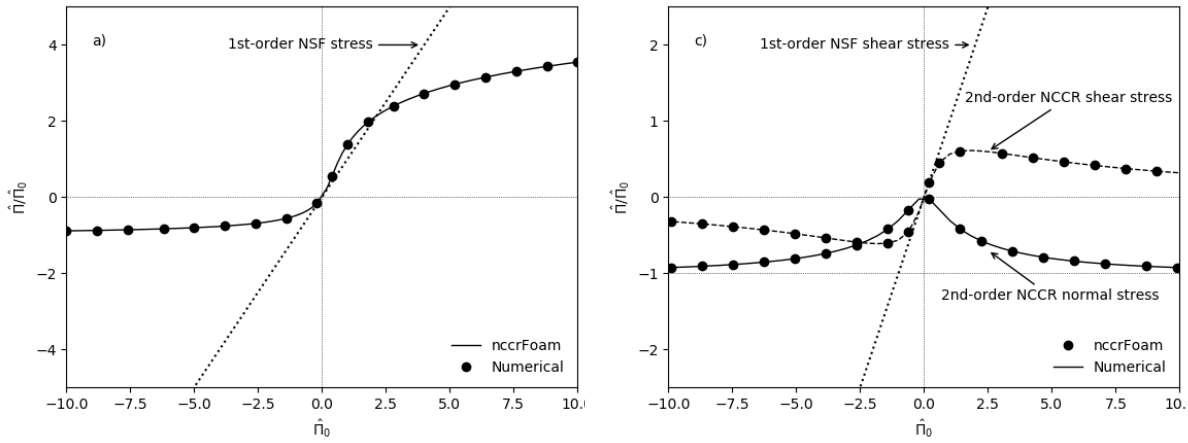

Fig. 3. Comparison of the cross-section of the topology: a) viscous normal stress ($\hat{\Pi}_{xx}$) for monoatomic gas flows (f_b = 0.0) as a function of the first-order normal stress-only case; and b) viscous normal and shear stress ($\hat{\Pi}_{xx}$ and $\hat{\Pi}_{xy}$) for monoatomic gas flows (f_b = 0.0), as a function of first-order shear-only stress employing *nccrFOAM* with previous numerically calculated results.

As explained in Subsection 3.1, the second-order NCCR can be solved at the cell interface by decomposing it into two sub-flows: the compression-expansion and the velocity-shear flows, according to the numerical technique developed by Myong [4]. In the previous verification study, we considered a 1D expansion-compression flow. Here we solve the 1D velocity-shear flows using the *nccrFOAM* solver. The input file for the velocity vector is initialized in such a manner that the normalized shear stress tensor in the *xy* and *yx* directions in the one-dimensional domain matches the values on the *x*-axis in Fig. 3c in reference [4]. Again, isothermal conditions are assumed, resulting in a non-heat flux case. For diatomic and polyatomic gases, an additional equation has to be included for the excess normal stress (Δ).

Fig. 3b shows a comparison of the normal and shear stresses calculated using the new *nccrFOAM* solver and those obtained using the method of iteration outlined in the previous literature [3] for argon gas. The results of the *nccrFOAM* solver perfectly match the previous results. It is interesting to note that even in velocity-shear-only flow, non-zero normal stress is present in the NCCR due to the coupled nature of the components of the viscous stress tensor, which is not possible in the case of NS constitutive laws. We also checked the second-order NCCR of diatomic and polyatomic gases with non-zero bulk viscosity ($f_b > 0$). The *nccrFOAM* solver reproduced a common kinematic viscous stress constraint in the results, whose topology is governed by a conic section and changes from an ellipse to a circle, to a parabola, and then finally to a hyperbola with increasing f_b, as shown in Fig. 4 [70].

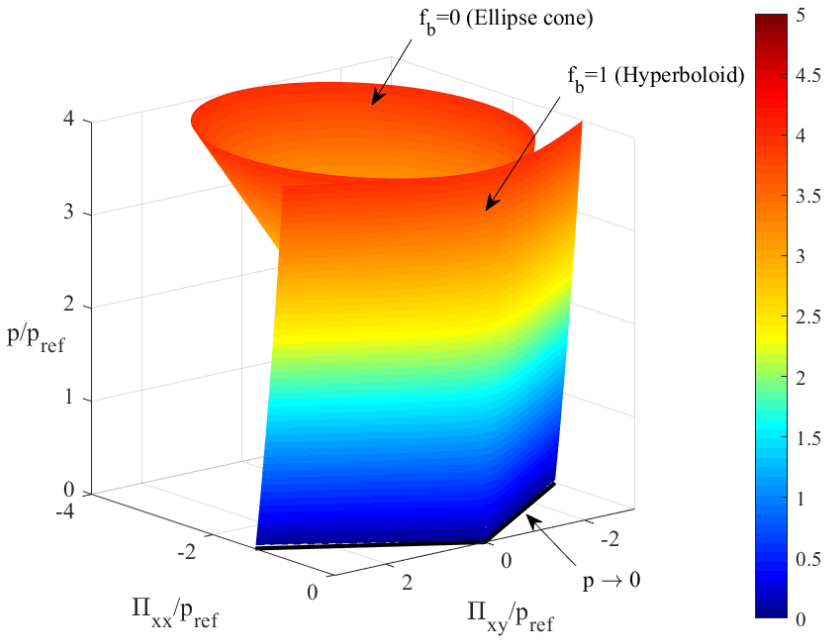

Fig. 4. Topology of the second-order Boltzmann-Curtiss-based constitutive models in the velocity shear flow problem in phase space (Π_{xx}, Π_{xy}, p) for $f_b = 0$ and $f_b = 1$. (Reproduced with permission from Singh et al., "Topology of the second-order constitutive model based on the Boltzmann–Curtiss kinetic equation for diatomic and polyatomic gases," Phys. Fluids 32, 026104 (2020). Copyright 2020 AIP)."

In addition, the *nccrFOAM* solver was verified on a two-dimensional domain. For instance, for monoatomic gases, $\hat{\Pi}_{xx}$ and $\hat{Q}_x$ are chosen as the relevant variables. The velocity and temperature components are initialized in the domain in such a manner that these values result in corresponding NSF values of viscous stress and heat flux. The second-order NCCR in *nccrFOAM* is solved iteratively to obtain the second-order viscous stress and heat flux. Again, the topological surfaces generated by the new solver perfectly matched those in the previous literature [70]. This verification study establishes the robustness and accuracy of the new *nccrFOAM* solver.

5.2 1D Shock structure simulation

Resolving the internal structure of a strong shock is considered to be one of the fundamental problems in the field of kinetic theory. Although limited, the availability of experimental data [71,72] in the form of inverse shock density thickness for monoatomic and diatomic gases is one of the reasons why shock structure simulations are widely used for validation studies. Several computational studies [20,69,71] based on first-order and higher-order methods in the Eulerian framework and even in the Lagrangian framework [72–74] have reported various

features of the internal shock structures for a wide variety of gases. Shock structure profiles based on nonlinear coupled constitutive relations have also been reported and discussed at length in several reports [3,39,52].

In the present work, shock structure simulations were performed for Maxwellian gases with a wide range of conditions using the new *nccrFOAM* and *nccrVibFOAM* solvers, and the shock profiles were compared with those obtained using the validated in-house FVM codes [52]. Stationary shock structure simulations were conducted for the following three cases:

- Mach 10 monoatomic argon gas flow using the *nccrFOAM* solver (single temperature NSF and NCCR with f_b = 0).
- Mach 10 nitrogen gas flow without vibrational non-equilibrium using the *nccrFOAM* solver (single temperature NSF and NCCR with f_b = 0.8).
- Mach 15 nitrogen gas flow with vibrational non-equilibrium using the *nccrVibFOAM* solver (two-temperature NSF and NCCR with f_b = 0.8) with constant relaxation V-T model $\tau_v = Z_{V-T} \cdot \tau_c$ where Z_{V-T} is constant relaxation collision number (=50) and τ_c is the mean collision time.

The detailed explanation provided here refers to those required to design the Mach 10 shock structure simulation of argon gas using the *nccrFOAM* solver. The other two simulations can be similarly designed by extending the first simulation. The *0* time folder contains the initial and boundary conditions required for the simulation. To define the shock structure profile for monoatomic, diatomic, and polyatomic gases without vibrational non-equilibrium, the number of independent input variables is three: pressure, temperature, and *x*-directional velocity. In contrast, the simulation for diatomic and polyatomic gases with vibrational non-equilibrium will require an additional input variable: vibrational temperature besides trans-rotational temperature. In the case of shock structure simulation, writing the input files in the *0* folder can be automated after constructing a mesh using a pre-defined *setFields* function.

The *constant* folder contains files describing the computational grid (in *polyMesh* sub-folder). In the present work, a 1000-celled one-dimensional grid for the shock structure simulation, spanning over a domain with a total length equal to sixty times the mean free path defined using the upstream condition, was chosen for the Mach 10 argon gas flow simulation. The grid was generated using the in-built *blockMesh* utility. The *constant* folder also contains the details of the simulated gas and its properties (basic thermal properties in

transportProperties and turbulence properties). In the present work, the laminar flow was assumed, and the turbulence models and the associated property file were redundant since the new *nccrFOAM* currently does not include turbulence modeling.

Additionally, a new file named *atomProperties* contains the details of the power-law viscosity model, flow properties, and reference values required for non-dimensionalizing the second-order NCCR, and various flags for the model (`nccr = 0` for NSF equations and = `1` for NCCR). Upstream conditions were chosen as the reference values for the second-order NCCR simulations.

The *system* folder contains files that control the procedure of the simulation itself. The files are similar to those written for *dbnsTurbFoam* with a few minor editions. To simulate the Mach 10 argon gas, various schemes in the *fvSchemes* file have to be defined for the additional non-conserved variables (`div(Pi), div((Pi&U)), div(Q)`).

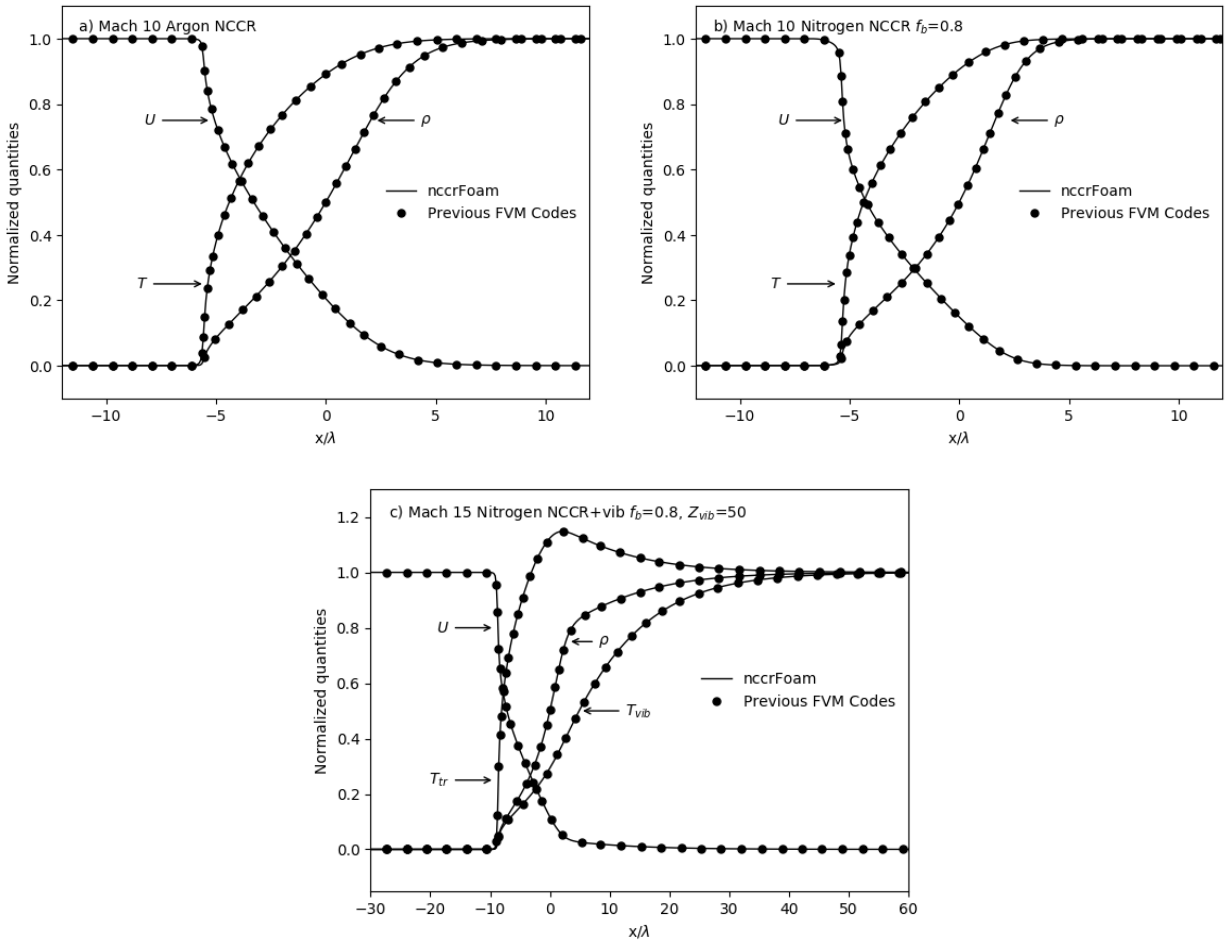

Fig. 5. Comparison of normalized properties (density, temperature, and *x*-directional velocity) as a function of normalized length: a) Mach 10 shock structure of argon gas; b) Mach 10 shock structure of nitrogen gas; and c) Mach 15 shock structure of nitrogen gas with vibrational non-equilibrium calculated using the new *nccrFOAM* solver and previous FVM codes.

The shock structure simulations for the three cases can be performed using either the first-order NSF or the second-order NCCR solvers. A first-order *nccrFOAM* simulation of monoatomic gas flows is equivalent to a *dbnsTurbFOAM* simulation. When first-order constitutive relations are used to simulate diatomic and polyatomic gas flows at low temperatures, the effect of bulk viscosity is effectively reflected in the governing equations, resulting in a system equivalent to the Navier-Fourier (NF) equation. It is noteworthy that the new *nccrFOAM* solver has the additional capability of handling the NF simulations, which is not possible with the existing *dbnsTurbFoam* solver. In addition, the new *nccrVibFOAM* solver solves diatomic and polyatomic gas flows with vibrational non-equilibrium at a higher temperature in a two-temperature framework, which is also unavailable in the current *dbnsFoam* or *dbnsTurbFoam* solvers. Shock structure simulations using the first-order constitutive relations were performed in the *nccrFOAM* solver and compared with the results obtained using the in-house FVM codes.

Fig. 5 compares normalized shock structure profiles obtained using the *nccrFOAM* solver and the previous FVM code as a function of normalized length for the Mach 10 shock structure of argon gas, Mach 10 shock structure of nitrogen gas, and Mach 15 shock structure of nitrogen gas with vibrational non-equilibrium. The *nccrFOAM* results are again in excellent agreement with those calculated with the FVM code. The profiles of not only conserved but also non-conserved variables were found to match very well in all three simulations.

5.3 Multi-dimensional NCCR simulations

Flow past a cylinder is a benchmark problem to validate new multi-dimensional solvers. In the present study, a hypersonic flow with Mach number 5.48 was simulated for Knudsen number 0.05 based on the diameter of a cylinder. The properties of the argon gas were as follows: gas constant R =208.24 *J*/*kg*/*K*, specific heat at constant pressure C_p =520.0 *J*/*K*, reference coefficient of viscosity μ_{ref} =2.117×10−5 *Pa s* at a reference temperature T_{ref} =273.15 *K*, index of viscosity power-law model ω =0.75, and Prandtl number *Pr* =2/3. The free-stream velocity of the gas along the *x*-direction (U_∞), ambient pressure (p_∞), and temperature (T_∞) were 526.3 *m*/*s*, 5 *Pa*, and 26.6 K, respectively. As argon is monoatomic gas, the bulk viscosity was set to zero, and the excess normal stress vanishes. The wall temperature (T_w) of the stationary cylinder was maintained at 293.15 *K*. The Maxwell velocity slip

condition and Smoluchowski temperature jump condition with full surface accommodation (α = 1) were assumed to be the wall boundary condition of the cylinder. To improve the convergence of the second-order NCCR solver, the new solver *nccrFoam* was used to simulate the first-order constitutive relations first. After convergence, the final results were used as input to the second-order NCCR solver.

Fig. 6 compares normalized density and temperature along the normalized stagnation line obtained by the first and second-order constitutive relations in the new *nccrFOAM* solver with those predicted by DG-NSF and DG-NCCR codes of Le *et al*. [39] and results obtained using the in-house DSMC code [75]. The present first-order NSF results match well with the corresponding DG-NSF results. The present second-order NCCR results also match well with the DG-NCCR results and DSMC. Interestingly, the present second-order NCCR results seem to be in better agreement with the DSMC compared to the DG-NCCR results. The deviation between the present *nccrFOAM* solver and DG-NCCR solver may be attributed to the different boundary treatment—Maxwell- Smoluchowski vs Langmuir—and the much finer grid resolution of the present work than that of Le *et al*. [39].

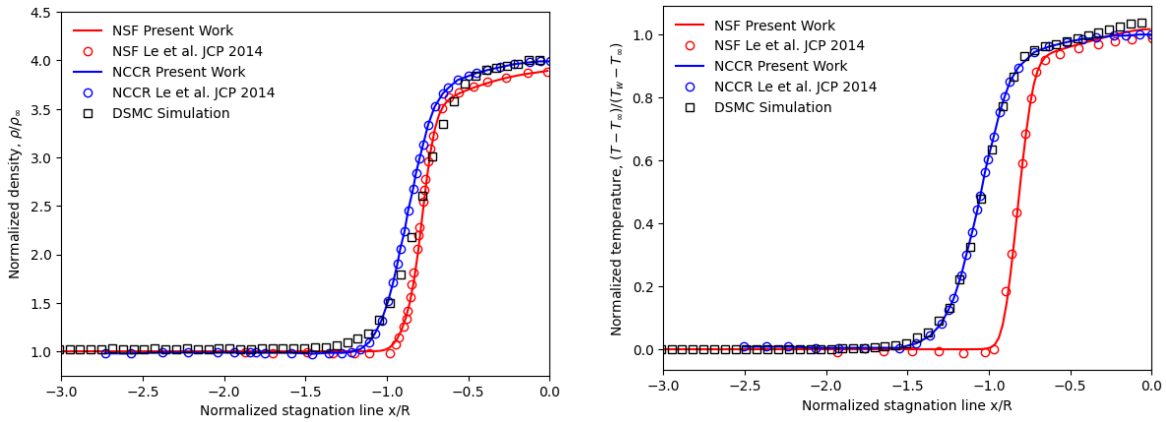

Fig. 6. Comparison of shock structure profiles along normalized stagnation line obtained with the first-order NSF and second-order NCCR solvers (present and DG), and DSMC for Mach 5.48 argon gas flow (Kn=0.05): a) normalized density; and b) normalized temperature.

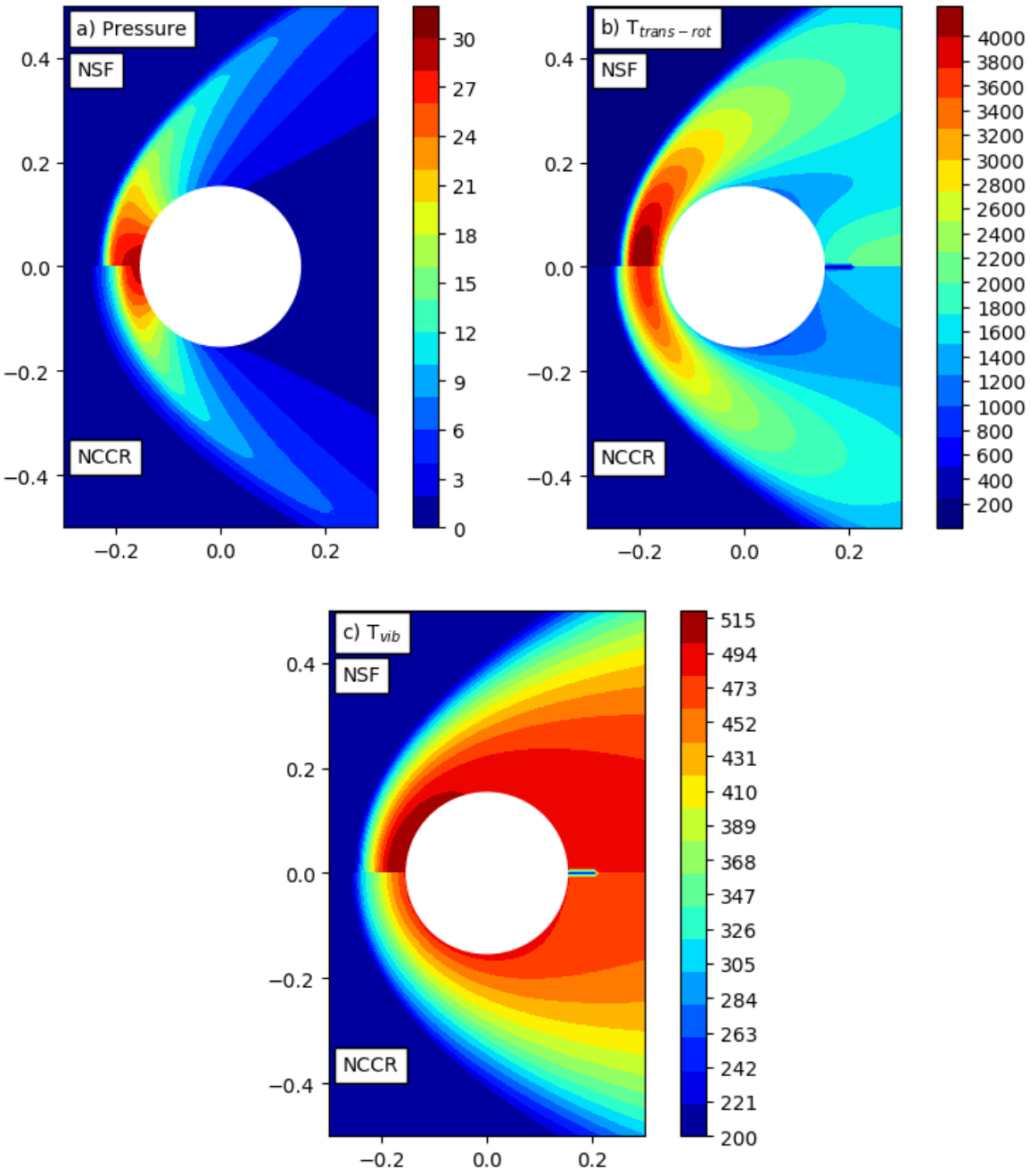

Fig. 7. Comparison of contours obtained with the first-order NSF and second-order NCCR using the *nccrVibFOAM* solver for Mach 10 nitrogen gas flow (Kn=0.05): a) pressure (Pa); b) trans-rotational temperature (K); and c) vibrational temperature (K).

The simulation of nitrogen gas flows with vibrational non-equilibrium in a two-temperature framework was also carried out using the *nccrVibFOAM* solver. The chosen Mach number and Knudsen number were 10 and 0.05, respectively. The ambient temperature, pressure, and *x*-direction velocity were set to 200 *K*, 0.2345 *Pa*, and 2883 *m*/*s*, respectively. The surface

temperature of the cylinder was set to 500 K. The Millikan-White vibrational relaxation model with Park's correction was employed to handle the vibrational non-equilibrium. The values of the constants A, B, σ were set to 220 $K^{1/3}$, -13.27, and 5.81×10^{-21} m^2, respectively.

Two simulations were performed with the first-order NSF and second-order NCCR solvers. For the NCCR simulation, the bulk viscosity ratio was set to f_b =0.8. Similar to the argon case, converged NSF solutions were taken as inputs to the NCCR simulation to improve the convergence. The Maxwell velocity slip condition and Smoluchowski temperature jump condition with full surface accommodation (α = 1) were assumed at the cylinder wall.

Fig. 7 compares contours of pressure, trans-rotational and vibrational temperatures obtained by the first-order NSF and second-order NCCR. The overall shock structure and distribution of flow properties in the flow field show significant differences. The shock thickness of the second-order NCCR is greater than that of the first-order NSF. The peak trans-rotational temperature of the second-order NCCR is significantly lower than that of the first-order NSF. The higher trans-rotational temperature of the first-order NSF in turn drives faster vibrational relaxation, leading to much higher vibrational temperatures compared to the second-order NCCR. This is consistent with our previous observation in the 1D shock structure analysis [52].

We present here for the first time the results of the second-order NCCR with vibrational non-equilibrium in a two-temperature framework for 2D hypersonic rarefied flow simulation. A parametric study of hypersonic rarefied nitrogen flows with vibrational non-equilibrium past various 2D bodies at varying Knudsen and Mach numbers, an analysis of the flow properties predicted by the NSF and NCCR, and a comparison with appropriate DSMC simulations are currently in progress and will be reported in the future.

The *nccrFOAM* solver can also be employed to investigate microscale gas flow applications. A two-dimensional steady-state Poiseuille flow of compressible argon gas through a micro-channel was considered. The laminar flow was induced by the pressure difference (the inlet and outlet pressures, P_{in} =1.2 *atm* and P_{out} = 0.5 *atm*, respectively) imposed on the channel with the length L = 8 μm and height H = 1 μm. The walls of the channel were maintained at a constant temperature T_w equal to the upstream flow temperature T_{in} =300 *K*. The Maxwell velocity slip and Smoluchowski temperature jump conditions with full momentum and thermal accommodation were imposed on the wall of the micro-channel. The flow velocity generated by the pressure difference varied in both the *x* and *y* directions, making this flow a multi-

dimensional problem. The results obtained using the first NSF and second-order NCCR of the *nccrFOAM* solver were compared with a suitably designed DSMC result [76–78].

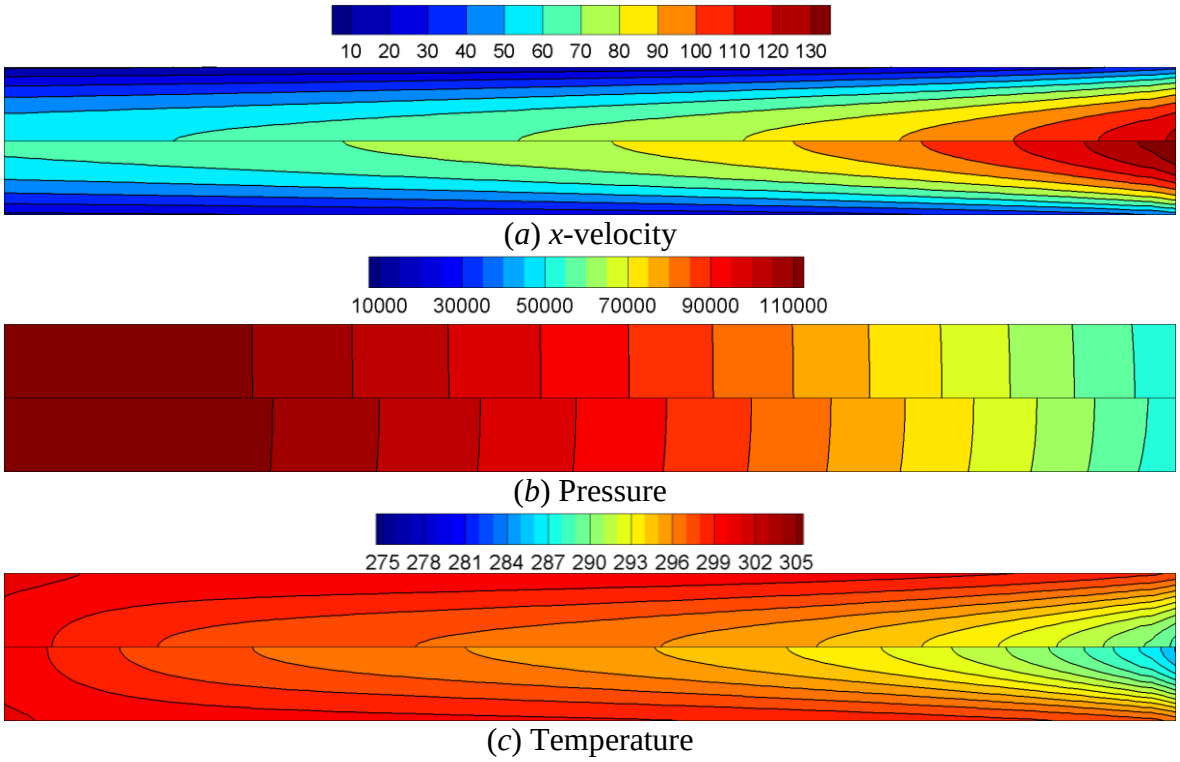

Fig. 8. Comparison of contours of primitive variables obtained using the first-order NSF (top) and second-order NCCR (bottom): a) *x*-velocity (m/s); b) pressure (Pa), and c) temperature (K).

Fig. 8 shows the contours of the NSF and NCCR results for the primitive variables. Fig. 9 compares the distribution of the *x*-directional velocity along with the channel height at three different sections of the channel, 0.2L, 0.5L, and 0.8L, respectively, as obtained with NSF, NCCR, and DSMC. The second-order NCCR results are in very good agreement with the DSMC data, especially at the center of the channel, even in the downstream section of the microchannel where rarefaction effects are dominant. However, the agreement decreases near solid walls where the flow is mainly affected by the velocity slip and temperature jump boundary conditions. Therefore, the disparity observed can be attributed to the dominance of the slip and jump models in that region. This mismatch at the wall has been reported in the previous work by Myong [79]. It was found that the NCCR model predicts higher slip compared to those predicted by the DSMC method. The results reported in the present work conform to this observation.

In addition to the micro-Poiseuille gas flows, the new solver can be employed to investigate other micro-channel applications [80] such as micro-Couette, cylindrical Couette, and cavity flow.

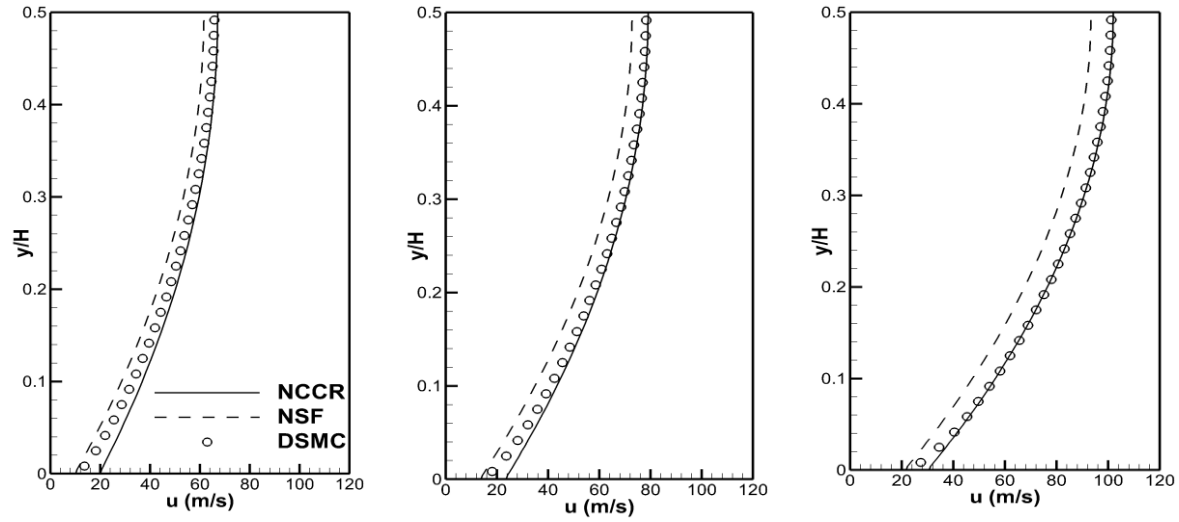

Fig. 9. Comparison of the *x*-directional velocity along the height at different locations in the microchannel obtained with NSF, NCCR, and DSMC: 0.2L (left); 0.5L (center); and 0.8L (right).

Finally, a challenging three-dimensional flow was investigated to evaluate the performance of the *nccrFOAM* solver. The problem undertaken was a 3D nozzle jet gas flow impinging onto a surface at near-vacuum, which represents the descent phase of a lunar landing [81]. A schematic of the domain and boundary conditions is shown in Fig. 10. The nozzle configuration is identical to that of the Apollo descent module. To save computational cost, a quarter of the domain was simulated. The computational grid consists of 136,000 hexagonal elements.

Fig. 11 shows the line plots along *x*- and *z*-coordinate and density isosurfaces colored by the Rayleigh-Onsager number (that is, a Rayleigh-Onsager dissipation function in a non-dimensional form, (10) or (14)) for two different cases. In both cases, the ambient pressure is set to near-vacuum condition (P_{amb} = 0.1 Pa). Figs. 11 (a)-(d) represent the case where the inlet pressure P_{in} is set to 100 Pa (a pressure ratio of 1000), while Figs. 11 (e)-(h) correspond to an inlet pressure of 10 Pa (a pressure ratio of 100). Similarly, Fig. 12 shows the variation of pressure, shear stress, and heat flux along the z-coordinate for the two cases (Figs 12. (a)-(c) at P_{in} = 100 Pa and pressure ratio of 1000, Figs. 12 (d)-(f) at P_{in} = 10 Pa and pressure ratio of 100). The NSF and NCCR solvers were used to solve both scenarios. The NSF solution under-predicted the location of the reflected shock (consequently, the stand-off shock position). The

gap between the two models was even greater when the inlet pressure was reduced (an increase in rarefaction effects).

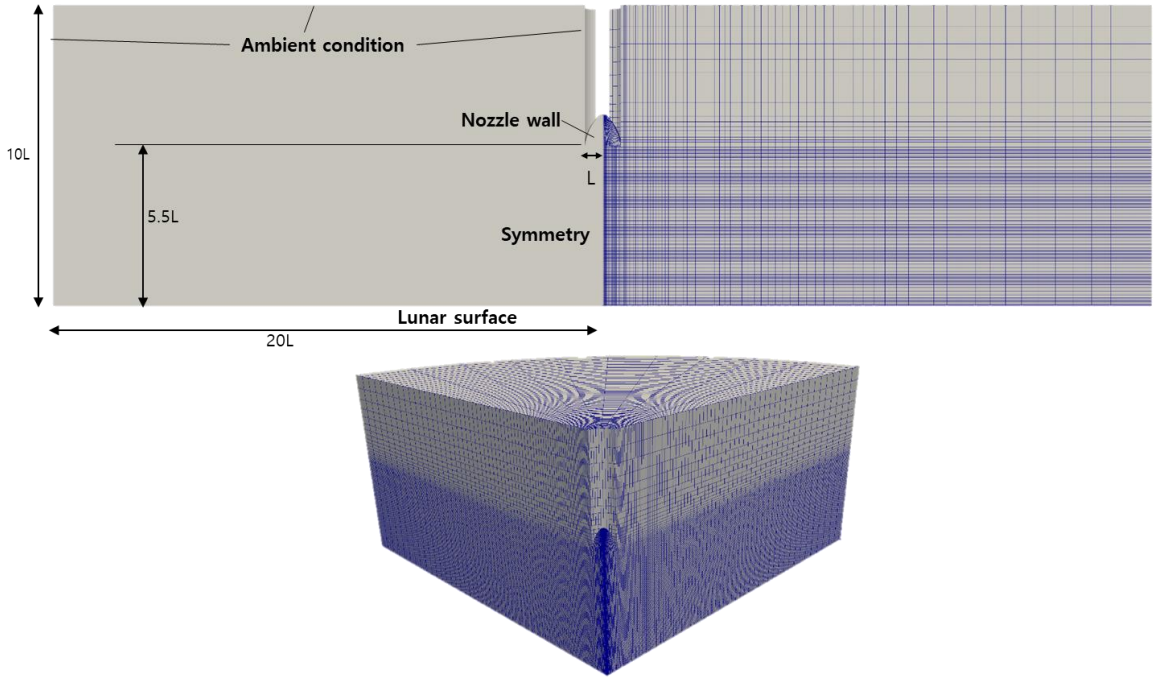

Fig. 10. Schematic drawing of the domain (and quarter domain) and boundary conditions.

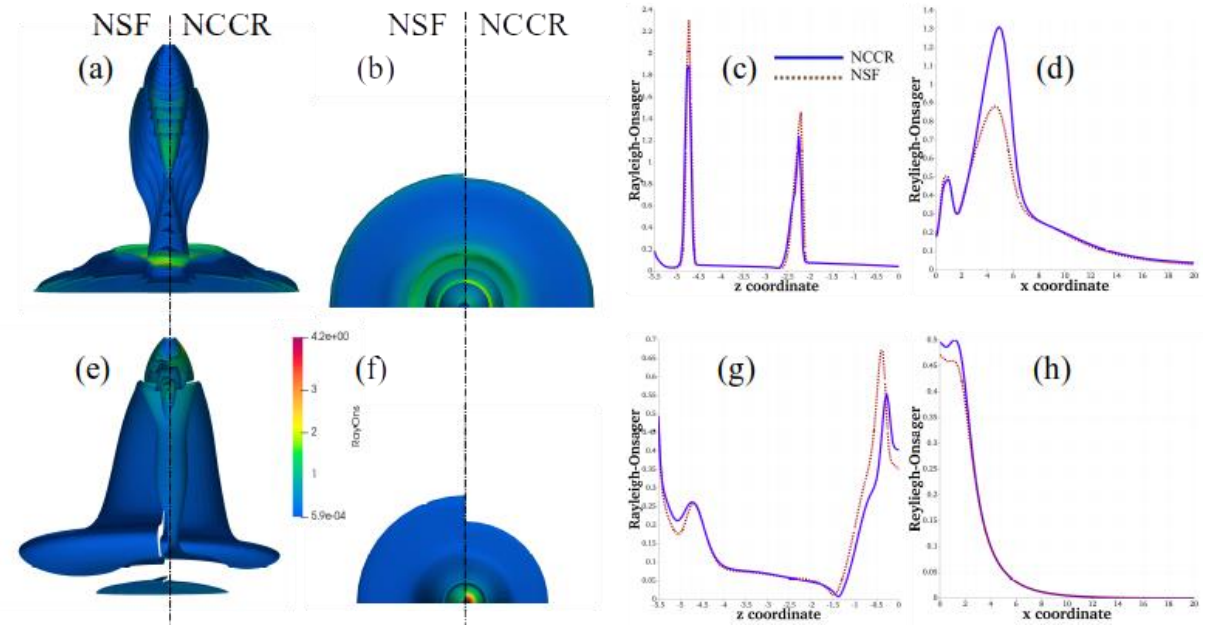

Fig. 11. Density isosurfaces colored by Rayleigh-Onsager number: a) and b) at P_{in}=100 Pa and pressure ratio=1000; e) and f) at P_{in}=10 Pa and pressure ratio=100, and, line plots for Rayleigh-Onsager number along the c) *z*- and d) *x*-coordinate at P_{in}=100 Pa and pressure ratio=1000; and along the g) *z*- and h) *x*-coordinate at P_{in}=10 Pa and pressure ratio=100, respectively.

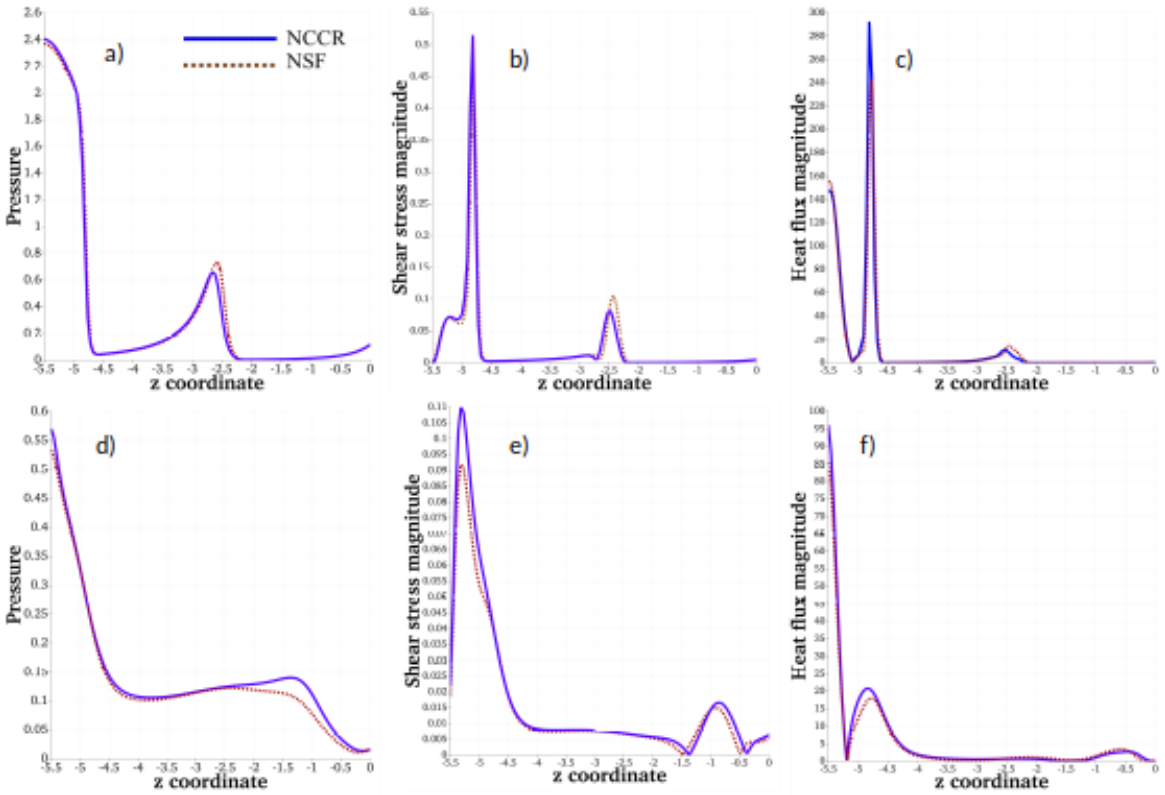

Fig. 12. Line plots along the *z*-coordinate for a) pressure, b) shear stress, and c) heat flux at P_{in}=100 Pa and pressure ratio=1000; d) pressure, e) shear stress, and f) heat flux at P_{in}=10 Pa and pressure ratio=100, respectively.

6. Conclusions and remarks

The *nccrFOAM* suite was developed to simulate rarefied and microscale gas flows using second-order constitutive relations for a wide range of applications. In particular, the new solver is capable of simulating rarefied gas flows with vibrational non-equilibrium using a two-temperature framework and state-of-the-art second-order constitutive relations developed from a modified Boltzmann-Curtiss kinetic equation for high non-equilibrium situations. Overall, *nccrFOAM* is a broad framework that can be utilized for a wide range of applications from shock structure simulations to hypersonic flows to microscale gas applications. The case files of several flow simulations including a shock structure problem with vibrational non-equilibrium, a hypersonic rarefied gas flow past a cylinder with/without vibrational non-equilibrium, and a 3D nozzle jet gas impinging onto a surface at near-vacuum are provided along with the code as a set of tutorials.

The present framework can easily be extended to investigate other important gas flows in high non-equilibrium such as the multi-phase flows and nozzle gas flows of thrusters working in space. A study on the development of second-order NCCR for hypersonic gas flows with the inclusion of chemical reactions is also currently in progress. The interplay between the various physical mechanisms—second-order trans-rotational, vibrational, and chemical non-equilibrium effects—will reveal a comprehensive description of complicated aerothermodynamic flows, such as the shock-dominated regions encountered in re-entry flows. Flow chemistry with the new set of equations will be added later to the current *nccrFOAM* framework.

The second-order NCCR theory is a complex subject that often presents barriers to entry in the field of rarefied and microscale gas flows with vibrational and chemical non-equilibrium. *nccrFOAM* is intended to provide a solution to assist these efforts. We hope that it is useful to the rarefied and microscale gas dynamics and hypersonics communities at large.

Acknowledgments

This work was supported by the National Research Foundation of Korea funded by the Ministry of Science and ICT (2022M1A3C2074536 Future Space Education Center, NRF 2022M1A3B8075129, and NRF 2017R1A5A1015311), South Korea. TKM would like to acknowledge the National Supercomputing Mission (DST/NSM/R&D_HPC_ Applications/2021/43) for the DSMC simulations performed in this work.

The authors would like to express their deepest gratitude to Professor Emeritus B. C. Eu of McGill University for his inspiration and encouragement in our research, who passed away last August.

References

[1] R.S. Myong, K. Xu, International Journal of Computational Fluid Dynamics 35 (8) (2021) 563–565.

[2] R.S. Myong, Physics of Fluids 26 (2014) 056102.

[3] R.S. Myong, Physics of Fluids 11 (1999) 2788–2802.

[4] R.S. Myong, Journal of Computational Physics 168 (2001) 47–72.

[5] C. Park, Nonequilibrium Hypersonic Aerothermodynamics, Wiley, New York, 1989.

[6] X. He, L.S. Luo, Physical Review E 55 (1997) 6811–6817.

[7] S. Chen, G.D. Doolen, Annual Review of Fluid Mechanics 30 (1998) 329–364.

[8] G.A. Bird, Annual Review of Fluid Mechanics 10 (1978) 11–30.

[9] G.A. Bird, Molecular Gas Dynamics and the Direct Simulation of Gas Flows, 2nd Edition, Clarendon Press, Oxford, 1994.

[10] G.A. Bird, Computers and Mathematics with Applications 35 (1998) 1–14.

[11] R.S. Myong, A. Karchani, O. Ejtehadi, Physics of Fluids 31 (2019) 066101.

[12] C. White, M.K. Borg, T.J. Scanlon, S.M. Longshaw, B. John, D.R. Emerson, J.M. Reese, Computer Physics Communications 224 (2018) 22–43.

[13] I.D. Boyd, T.E. Schwartzentruber, Nonequilibrium Gas Dynamics and Molecular Simulation, University Press, Cambridge, 2017.

[14] D. Burnett, Proceedings of the London Mathematical Society 2 (1936) 382–435.

[15] N. Singh, N. Dongari, A. Agrawal, Microfluidics and Nanofluidics 16 (2014) 403–412.

[16] N. Singh, R.S. Jadhav, A. Agrawal, Physical Review E 96 (2017) 013106.

[17] M.S. Shavaliyev, Journal of Applied Mathematics and Mechanics 57 (1993) 573–576.

[18] K. Xu, Physics of Fluids 15 (2003) 2077–2080.

[19] K.A. Fiscko, D.R. Chapman, International Symposium on Rarefied Gas Dynamics: Theoretical and Computational Techniques, 1989.

[20] M. Torrilhon, H. Struchtrup, Journal of Fluid Mechanics 513 (2004) 171–198.

[21] N. Singh, A. Agrawal, Physical Review E 93 (2016) 063111.

[22] B.C. Eu, The Journal of Chemical Physics 73 (6) (1980) 2958–2969.

[23] B.C. Eu, The Journal of Chemical Physics 74 (5) (1981) 3006–3015.

[24] B.C. Eu, Accounts of Chemical Research 19 (1986) 153–160.

[25] B.C. Eu, Kinetic Theory and Irreversible Thermodynamics, Wiley-Interscience, 1992.

[26] M. Al-Ghoul, B.C. Eu, Physical Review E 56 (1997) 2981–2992.

[27] T. Arima, S. Taniguchi, T. Ruggeri, M. Sugiyama, Continuum Mechanics and Thermodynamics 24 (2012) 271–292.

[28] S. Taniguchi, T. Arima, T. Ruggeri, M. Sugiyama, Physical Review E 89 (2014) 013025.

[29] T. Ruggeri, M. Sugiyama, Rational Extended Thermodynamics beyond the Monatomic Gas, Springer, Cham, 2015.

[30] T. Arima, A. Mentrelli, T. Ruggeri, Annals of Physics 345 (2014) 111–140.

[31] V. Kolobov, R. Arslanbekov, V. Aristov, A. Frolova, S.A. Zabelok, Journal of Computational Physics 223 (2) (2007) 589–608.

[32] K. Xu, J. Huang, Journal of Computational Physics 229 (20) (2010) 7747–7764.

[33] L. Zhu, Z. Guo, K. Xu, Computers & Fluids 127 (2016) 211–225.

[34] A. Peng, Z. Li, J. Wu, X. Jiang, Journal of Computational Physics 327 (2016) 919–942.

[35] Z. J. Liu, C. Shu, S.Y. Chen, L.M. Yang, M.P. Wan, W. Liu, Journal of Computational Physics 415 (2020) 109548.

[36] C.J. Lee, AIAA Journal 32 (5) (1994) 985–990.

[37] R.S. Myong, Journal of Computational Physics 195 (2004) 655–676.

[38] M. Al-Ghoul, B.C. Eu, Physical Review E 64 (2001) 046303.

[39] N.T.P. Le, H. Xiao, R.S. Myong, Journal of Computational Physics 273 (2014) 160–184.

[40] L.P. Raj, S. Singh, A. Karchani, R.S. Myong, Computers & Fluids 157 (2017) 146–163.

[41] T. Chourushi, S. Singh, V. Asokakumar Sreekala, R.S. Myong, International Journal of Computational Fluid Dynamics 35 (8) (2021) 565–592.

[42] S. Singh, A. Karchani, T. Chourushi, R.S. Myong, Journal of Computational Physics 457 (2022) 111052.

[43] T. Chourushi, A. Rahimi, S. Singh, O. Ejtehadi, T. K. Mankodi, R.S. Myong, International Journal of Heat and Mass Transfer 187 (2022) 122580.

[44] J.W. Ahn, C. Kim, Journal of Computational Physics 228 (2009) 4088–4117.

[45] Z. Jiang, W. Zhao, Z. Yuan, W. Chen, R.S. Myong, AIAA Journal 57 (2019) 5252–5268.

[46] Z. Jiang, W. Zhao, W. Chen, R.K. Agarwal, Shock Waves 29 (2019) 1227–1239.

[47] Z. Jiang, W. Zhao, W. Chen, R.K. Agarwal, Communications in Computational Physics 26 (3) (2019) 880–912.

[48] Z. Yuan, W. Zhao, Z. Jiang, W. Chen, Aerospace Science and Technology 112 (2021) 106591.

[49] C.F. Curtiss, The Journal of Chemical Physics 75 (1981) 376–378.

[50] B.C. Eu, Y.G. Ohr, Physics of Fluids 13 (2001) 744–753.

[51] F.R.W. McCourt, J.J.M. Beenakker, W.E. Köhler, I. Kuščer, Nonequilibrium Phenomena in Polyatomic Gases: Volume 1 Dilute Gases, Clarendon Press, Oxford, 1990.

[52] T.K. Mankodi, R.S. Myong, Physics of Fluids 32 (2020) 126109.

[53] D.R. White, R.C. Millikan, AIAA Journal 2 (1964) 1844–1846.

[54] R.N. Schwartz, Z.I. Slawsky, K.F. Herzfeld, The Journal of Chemical Physics 20 (1952) 1591–1599.

[55] L. Onsager, Physical Review 37 (1931) 405–426.

[56] R.S. Myong, Physics of Fluids 16 (2004) 104–117.

[57] R.S. Myong, Physics of Fluids 23 (2011) 012002.

[58] R.S. Myong, Physics of Fluids 28 (2016) 012002.

[59] J.C. Maxwell, Philosophical Transactions of the Royal Society 170 (1879) 231–256.

[60] M. Smoluchowski von Smolan, Annalen Der Physik 300 (1898) 101–130.

[61] C.J. Greenshields, H.G. Weller, L. Gasparini, J.M. Reese, International Journal for Numerical Methods in Fluids 63 (2010) 1–21.

[62] A. Kurganov, E. Tadmor, Journal of Computational Physics 160 (2000) 241–282.

[63] A. Kurganov, S. Noelle, G. Petrova, SIAM Journal on Scientific Computing 23 (2002) 707–740.

[64] E.F. Toro, Riemann Solvers and Numerical Methods for Fluid Dynamics, 2nd Edition, Springer Science & Business Media, 2009.

[65] E.F. Toro, M. Spruce, W. Speares, Shock Waves 4 (1994) 25–34.

[66] H. Luo, J.D. Baum, R. Löhner, Journal of Computational Physics 194 (2004) 304–328.

[67] P.L. Roe, Journal of Computational Physics 43 (1981) 357–372.

[68] V.V. Rusanov, J. Comput. Math. Phys. USSR 1 (1961) 304–320.

[69] J.M. Reese, L.C. Woods, F.J.P. Thivet, S.M. Candel, Journal of Computational Physics 117 (1995) 240–250.

[70] S. Singh, A. Karchani, K. Sharma, R.S. Myong, Physics of Fluids 32 (2020) 026104.

[71] R.S. Myong, AIAA Journal 52 (2014) 1075–1081.

[72] F. Fei, H. Liu, Z. Liu, J. Zhang, AIAA Journal 58 (2020) 2596–2608.

[73] P. Valentini, C. Zhang, T.E. Schwartzentruber, Physics of Fluids 24 (2012) 106101.

[74] G.V. Shoev, M.Y. Timokhin, Y.A. Bondar, Physics of Fluids 32 (2020) 041703.

[75] T.K. Mankodi, U.V. Bhandarkar, B.P. Puranik, Acta Astronautica 162 (2019) 243–255.

[76] O. Ejtehadi, E. Roohi, J.A. Esfahani, International Communications in Heat and Mass Transfer 39 (2012) 439–448.

[77] A. Karchani, O. Ejtehadi, R.S. Myong, Communications in Computational Physics 20 (5) (2016) 1183–1209.

[78] J.A. Esfahani, O. Ejtehadi, E. Roohi, International Journal of Exergy 13 (2013) 320–342.

[79] R.S. Myong, Physics of Fluids 28(1) (2016) 012002.

[80] T. Chourushi, S. Singh, R.S. Myong, Journal of Computational Fluids Engineering 23 (2018) 62–71.

[81] O. Ejtehadi, R.S. Myong, Journal of Computational Physics 411 (2020) 109410.